Chapter 1

Introduction

1.1 Perspectives in smart structures

The field of smart structures has been an emerging area of research for the last few decades. Smart structures (also called smart material structures) can be defined as structures that are capable of sensing and actuating in a controlled manner in response to a stimulus [BSW96]. The development of this field is supported by the development in the field of materials science and in the field of control. In materials science, new smart materials are developed that allow them to be used for sensing and actuation in an efficient and controlled manner. These smart materials are to be integrated with the structures so they can be employed as actuators and sensors effectively. It is also clear that the field of smart structures also involves the design and implementation of the control systems on the structures. A well designed and implemented controller for smart structures is thus desirable.

In this thesis, we consider the case of vibration of smart structures. The stimulus to a structure may originate from external disturbances or excitations that cause structural vibrations. A smart structure would be able to sense the vibration and generate a controlled actuation to itself so the vibration can be minimized. For vibration control purposes, a number of smart materials can be used as actuators and sensors such as piezoelectric, shape memory, electrostric-

tive and magnetostrictive materials. Here, we concentrate on using piezoelectric materials because they have good broadband sensing and actuation properties.

In 1880, Pierre and Paul-Jacques Curie discovered the direct piezoelectric effect on various crystals such as tourmaline, Rouchelle salt and quartz. The crystals generated electrical charges on their surfaces when they were mechanically strained in certain directions. In the following year, they also discovered the converse piezoelectric effect, that the shape of crystals would change when an electric field was applied to them.

The ability of the piezoelectric materials to exchange electrical and mechanical energy opens up the possibility of employing them as actuators and sensors. If the piezoelectric materials are bonded properly to a structure, structural deformations can be induced by applying a voltage to the materials, employing them as actuators. On the other hand, they can be employed as sensors since deformations of a structure would cause the deformed piezoelectric materials to produce an electric charge. The extent of structural deformation can be observed by measuring the electrical voltage the materials produce. Unfortunately, the piezoelectric effect in natural crystals is rather weak so they cannot be used effectively as actuators or sensors.

However, recent developments in the field of materials science has provided piezoelectric materials that have sufficient coupling between electrical and mechanical domains. Two of the commonly used piezoelectric materials are polyvinylidene fluoride (PVDF), a semicrystalline polymer film, and lead zirconate titanate (PZT), a piezoelectric ceramic material. PZT has larger electromechanical coupling coefficients than PVDF so PZT can induce larger forces or moments on structures. However, PZT is relatively brittle while PVDF is flexible and can be easily cut into any desired shape. PVDF also has good sensing properties so it is commonly used for sensors. In this thesis, we concentrate on using PZT as actuators and sensors. Our experiments show that PZT can be effectively used as a transducer for vibration control of flexible structures.

The linear relationship that governs the direct and converse piezoelectric effects can be expressed as [BSW96, GT92]:

$$\begin{aligned} D &= e^T\ S + \alpha^s\ E \\ \sigma &= c^E\ S - e\ E \end{aligned} \tag{1.1}$$

where D, E, S and σ are the electric displacement, electric field, strain and stress vectors respectively. Further, e, α^s and c^E are the dielectric permittivity matrix, dielectric matrix at constant mechanical strain and elastic coefficient matrix at constant electric field respectively. However, for piezoelectric laminate structures that are used in our research, it is sufficient to use the simplified form of the formulation.

In smart structures, there are several issues that need to be addressed such as the modelling, placement of actuators and sensors, and controller design. The modelling of smart structures does not just involve the modelling of flexible structures, but also includes the modelling of the smart materials used as actuators and sensors. For piezoelectric laminate structures, the derivations of equations of motion involve the modelling of forces or moments generated by the bonded piezoelectric actuators. Tzou [Tzo89], Lee [Lee87] and Lee and Moon [LM90] provide comprehensive electromechanical properties of piezoelectric materials. The modelling of such structures has been explored by a number of researchers [Lee90, DFR91, FEN96, CSG98, PA95, LM89, CdL87]. In some cases, it can be reasonably assumed that the piezoelectric patches do not change the original structural mass and stiffness properties. This is due to the fact that many piezoelectric patches used are relatively thin and lightweight compared to the main structure. Hence, a sufficient model of a piezoelectric laminate structure can still be achieved based on the assumption.

More complex modellings of piezoelectric laminate structures are discussed in [BSW96, Yu96], where they include the change in structural properties due to the piezoelectric patches. Banks *et al.* [BSW96] discuss the modellings of beams, plates and shells, while Yu [Yu96] concentrates on linear and non-linear

vibrations of plates. When the dimensions of the patches are considerable relative to those of the main structure, these modelling methods would be useful to obtain a more accurate model of the structure (see [TT90, TY96], for example).

The equations of motion of the structures can then be solved using a variety of modelling methods such as the modal analysis, Rayleigh-Ritz, assumed-modes, and finite element (FE) methods [CSG98, Mei75, Ros91, CL91]. For a structure with non-uniform structural properties, approximate methods like the FE method may be necessary to obtain the model of the system.

Alternatively, if the structure is already built, we can obtain its model directly from the structure via system identification . For instance, the information about the modal properties of the system can be obtained using the experimental modal analysis method, i.e. modal testings [SM99, Ewi84]. The results from the modal testings can be used to update the FE model of a structure using updating methods [Fri95, Fla98]. For example, the mass and stiffness matrices of the FE model can be updated by minimizing the norm of the error in modal properties. Hence, a realistic model can be obtained from such methods, although this can only be done when the structure already exists.

However, since the model of a flexible structure originally consists of a large number of resonant modes, a model reduction is often required. A number of approaches for model reduction have been developed, such as model reduction via balanced realization [GL95, SP96, MPP99]. However, since the approaches are generally based on the order reduction of a finite-dimensional model, there is a limit on how many high frequency modes can be included when a resonant system with a spatially distributed nature is considered.

The model order can also be reduced by direct truncation where higher frequency modes, i.e. out-of-bandwidth modes, are truncated. However, the removal of the out-of-bandwidth modes may affect the zero-frequency (DC) content and locations of the in-bandwidth zeros of the system, leading to truncation errors. The truncation errors can be minimized by adding a feedthrough term to the truncated model. The technique is known in the aeroelasticity literature

as the mode acceleration method [BA75]. In the mode acceleration method [Cla97, BA75], the feedthrough term only reduces the DC error to zero, while the error may increase with frequency. Moheimani [Moh00a, Moh00b] and Moheimani and Heath [MH00] suggest alternative approaches for finding the optimal feedthrough terms for models that are obtained from modal analysis. The optimal feedthrough terms are found by minimizing the norms of the error between the full-order model and truncated model. However, assuming the system damping is small, the effect of damping is not considered in the approaches. For systems with considerable damping, the obtained feedthrough terms may not be close to optimal anymore.

Apart from the modelling issue, the issue of optimal placement of actuators and sensors is also of considerable interest in the field of smart structures. It is important to place actuators or sensors on a structure at locations where they have sufficient authority to control or sense structural vibrations. Given the importance of optimal placement, a number of researchers have addressed this issue in the past. For instance, Gawronski [Gaw98, Gaw97] and Smith and Clark [SC01] address the problem of actuator and sensor placement based on Hankel singular values of the system. However, the approach depends on the assumption that the system damping is small, where the controllability and observability Gramians of the system can be shown to be diagonally dominant. For piezoelectric actuators and sensors, a variety of modal sensitivity or controllability/observability measures can also be used to determine their optimal placement on a flexible structure [CdL87, HCSL97, SWW98]. The optimal locations generally correspond to the locations of high average strain for each desired mode shape (see [SR96, BL96], for example). Other optimal placement approaches that exploit the controllability and observability Gramians of a system have also been explored [DMPB92, LAKB01].

Moheimani and Ryall [MR99] optimize the placement of piezoelectric actuators on beams using a spatial controllability measure. For this purpose, they define the spatial controllability and modal controllability measures. The modal

controllability measure defined here differs from those that are used in other references. The measure is based on the spatial $\mathcal{H}_2$ norm of a spatially distributed system introduced by Moheimani and Fu [MF98] that reflects on the total energy of the system. The concept of spatial $\mathcal{H}_2$ norm would be useful when dealing with spatially distributed systems such as flexible structures.

An alternative optimal placement approach is by integrating the placement of actuators and sensors with the controller design, for instance, by using the optimization of quadratic performance indexes [FW97, Dem00, DMPB92]. This means that the actuator and sensor locations would depend on the choice of controllers. However, when more than one controller are to be tested on the structure, it may not be practical to change the locations of actuators and sensors on the structure.

Another important issue in smart structures is the controller design for minimizing vibration of smart structures. A variety of control design frameworks for active control of flexible structures have been explored. Meirovitch [Mei87] discusses the Independent Modal-Space Control (IMSC) where each mode is controlled independently. However, this requires modal state estimation that may create spillover problem, as mentioned by Balas [Bal78b, Bal78a]. Balas [Bal79] discusses the use of direct velocity feedback control, where the closed-loop system is unconditionally stable in the absence of actuator dynamics. But instability may arise if the actuator dynamics is taken into account as pointed out by Goh and Caughey [GC85]. In general, position and velocity feedback control design (see [GC85, BKFK91, Cau95], for example) have been used for vibration control of piezoelectric laminate structures [SW97, WSBS92, YB96, GR89, Tzo91].

In modern control, the $\mathcal{H}_2$ and $\mathcal{H}_\infty$ control frameworks are well-known. The $\mathcal{H}_\infty$ control framework is particularly useful for robust control design since uncertainties in the model can be conveniently accounted for. The work of Doyle *et al.* [DGKF89] and Glover and Doyle [GD88] for obtaining state-space solutions to standard $\mathcal{H}_2$ and $\mathcal{H}_\infty$ control problems have been instrumental since optimal $\mathcal{H}_2$ and $\mathcal{H}_\infty$ controllers can be simply obtained from the solutions of

algebraic Riccati equations. Another alternative approach for solving $\mathcal{H}_2$ and $\mathcal{H}_\infty$ control problems is via a convex optimization, using the so-called Linear Matrix Inequality (LMI) approach [BEGFB94, GA93, Gah94, IS93].

However, spatially distributed systems have theoretically an infinite number of modes and are represented by infinite-dimensional models. To design a controller using the standard $\mathcal{H}_2$ and $\mathcal{H}_\infty$ control design frameworks, finite-dimensional models are required. Model order reduction is thus needed to obtain such finite-dimensional models. In addition, the problem of $\mathcal{H}_\infty$ control for spatially distributed systems has been addressed in the literature (such as in [LÖT$^+$91, LÖT$^+$89, LÖ93, ÖT90, ÖT91, SCF94]). For example, Lenz *et al.* [LÖT$^+$91, LÖT$^+$89] and Lenz and Özbay [LÖ93] suggest infinite-dimensional controllers that are obtained from the infinite-dimensional models. Finite-dimensional controllers are then approximated from the infinite-dimensional controllers.

In general, such as in [LÖT$^+$91, LÖT$^+$89, LÖ93, SCF94], the models used for control design describe vibrations at one or several locations along the structures, i.e. pointwise models. Thus, the controller is designed based only on the information of one or a few locations along the structure. However, vibration characteristics at other locations along the structure are not accounted for. This may cause problems if vibration reduction over the entire structure is needed.

To deal with such problems, Moheimani and Fu [MF98] use the concept of spatial $\mathcal{H}_2$ norm of a spatially distributed system. This is done by employing the spatial information embedded within the models of structures that result from the modal analysis. The spatial $\mathcal{H}_\infty$ norm of a spatially distributed system is also proposed in [MPP99, MPP98]. Both norms can be seen as natural extensions of $\mathcal{H}_2$ norm and $\mathcal{H}_\infty$ norm for spatially distributed systems. The optimal spatial $\mathcal{H}_2$ and $\mathcal{H}_\infty$ controllers can be conveniently obtained by finding the equivalent standard $\mathcal{H}_2$ and $\mathcal{H}_\infty$ control problems respectively. The spatial controllers obtained ensure vibration reduction over entire structures in a spatially-averaged

sense. However, the concepts have not been implemented on real systems in a thorough manner.

In relation to stability and robustness of closed-loop systems, the concept of passivity is well-known. Here, a passive system can be stabilized by a stable and strictly passive controller as suggested by Desoer and Vidyasagar [DV75]. For linear time-invariant (LTI) systems, a positive-real system would be passive. In general, many unconditionally stable closed-loop systems can be derived from this passivity theory. Other work in this area has also been done by Moylan and Hill [MJ78, DM80]. Later, Joshi and Gupta [JG96] discuss the stability of closed-loop systems using less restrictive definition of passivity. Other researchers have used this passivity approach to design feedback controllers [LLJ88, SS96, HBW94]. The requirement for a positive-real system can be obtained by collocating the actuators and sensors. For instance, the direct velocity feedback control mentioned previously can also be shown to make the closed-loop system passive [Bal82]. For a non-collocated system, a passification method may be applied to make the system passive (see [KJ97], for example).

1.2 Aims of the thesis

Considering the amount of research that have been done, this thesis is aimed at further exploring some issues in vibration analysis and control of smart structures, in particular piezoelectric laminate structures. In the area of vibration analysis, we wish to develop an efficient model correction approach for resonant systems that are obtained from modal analysis and approximate methods. Model correction for pointwise and spatial models of resonant systems would be considered. We wish to include the effect of damping in the resonant system, which are assumed to be negligible in other approaches. The developed model correction approaches would be able to be implemented on smart structure systems.

Moreover, we also explore the issue of optimal placement of actuators and sensors on flexible structures. We wish to develop an optimal placement methodology that works for general actuators and sensors. The methodology should be able to be implemented on a structure whose model can be obtained from a variety of modelling methods, such as from modal analysis and approximate methods. This would allow a realistic structure with complicated properties and boundary conditions to be considered. Consequently, we would also use this optimal placement methodology to optimally place piezoelectric actuators and sensors over a structure.

Finally, in vibration control of smart structures, we wish to investigate different types of active controllers for minimizing vibration of smart structures. We wish to develop controllers that are capable of minimizing vibration of the entire structure in a spatially-averaged sense. The proposed spatial controllers should also have sufficient robustness properties and can be implemented on real systems effectively. For these reasons, the spatial controllers would need to be implemented on real smart structure systems such as piezoelectric laminate beams.

1.3 Organization of the thesis

We organize the chapters in this thesis as follows:

Chapter 2: Modelling of smart structures

We consider the derivations of equations of motions for axial, torsional and flexural vibrations of beams and plates. We review some of common modelling methods: modal analysis, Rayleigh-Ritz, assumed-modes and FE methods. The modelling of piezoelectric laminate beams using modal analysis and FE methods are considered.

Chapter 3: Spatial norms

We discuss the concept of spatial norms for LTI spatially distributed systems. This concept will be used in the later chapters for model correction, optimal placement of actuators and sensors, and vibration control design. The spatial $\mathcal{H}_2$ norm and spatial $\mathcal{H}_\infty$ norm for such systems are defined in this chapter.

Chapter 4: Model correction

We consider several model correction approaches to compensate for the errors that arise from truncating high frequency dynamics from models of resonant systems. Optimal feedthrough terms are added to the truncated models to compensate for the truncation errors. We review the analytical solutions for optimal feedthrough terms for models that assume no damping in the systems. For systems with considerable damping, we propose an alternative approach for finding the optimal feedthrough terms numerically via a convex optimization. We also extend the previous analytical approach for models that include damping. Finally, we extend the proposed model correction approaches to include models that are obtained from approximate methods, such as from the FE method.

Chapter 5: Optimal placement of actuators and sensors

The optimal placement of actuators and sensors are discussed here. We extend the methodology for the actuator placement to reduce the effect of control spillover. A new method for optimal placement of sensors is proposed in this chapter. We consider the optimal placement of a collocated piezoelectric actuator/sensor pair on a thin plate and experimentally test the optimal placement results. We extend the optimal placement methodology to include models that are obtained from experimental modal analysis and approximate methods. As an illustrative example, we consider the optimal placement of a collocated piezoelectric actuator/sensor pair on a wing model.

Chapter 6: Resonant control

We propose a class of resonant controllers that can be implemented on structures with compatible pairs of collocated actuators and sensors. We introduce

a special class of robust resonant controllers that ensure closed-loop stability against parametric uncertainties and unmodelled dynamics in the model. An optimization procedure is developed to obtain the controller damping ratios so the spatial $\mathcal{H}_2$ norm of the closed-loop system is minimized. We design and experimentally implement the resonant controller on a piezoelectric laminate beam.

Chapter 7: Spatial $\mathcal{H}_2$ control

We extend the concept of spatial $\mathcal{H}_2$ norm for vibration control of smart structures. The spatial $\mathcal{H}_2$ controller is designed such that the spatial $\mathcal{H}_2$ norm of the closed-loop system is minimized. This ensures the structural vibration reduction in a spatially-averaged sense. The design and experimental implementation of the spatial $\mathcal{H}_2$ controller on a piezoelectric laminate beam are discussed.

Chapter 8: Spatial $\mathcal{H}_\infty$ control

We use the concept of spatial $\mathcal{H}_\infty$ norm to design and implement a spatial $\mathcal{H}_\infty$ controller for smart structures. We design the spatial $\mathcal{H}_\infty$ controller such that the spatial $\mathcal{H}_\infty$ norm of the closed-loop system is minimized. In this chapter, we discuss the design and experimental implementation of the controller to a piezoelectric laminate beam.

Chapter 9: Conclusions

We conclude the thesis by stating the main contributions of our research. Recommendations for further research in this area are also included.

Chapter 2

Modelling of smart structures

Before we can design a controller for minimizing structural vibration, we need to understand the vibration mechanism of the structure. Once the physical mechanism of vibration is understood, a good performance controller can be designed and implemented. This issue necessitates obtaining a sufficiently accurate physical model of a structure. The robustness of the controller can be affected considerably by the accuracy of the model in estimating the actual system.

Considering the significant role of modelling in control design of smart structures, we will discuss the modelling issue in this chapter. Smart structures considered in this thesis are flexible structures with smart material transducers attached to them. We concentrate on the use of piezoelectric materials as actuators and sensors due to their good performances as transducers.

Here, we will focus on LTI systems by considering that the structural vibrations are sufficiently small and the systems are assumed to be stationary. The piezoelectric transducers used are also operated in their linear operating region.

We will review some common modelling methods such as modal analysis, Rayleigh-Ritz, assumed-modes, and FE methods. However, smart structures that we deal with can be sufficiently modelled using the modal analysis method, although other modelling methods can also be used. Therefore, a greater proportion of this chapter will be reserved for the modelling of smart structures via modal analysis. The last three methods discussed here are approximate

methods, which are useful for modelling complicated systems with general boundary conditions and non-uniform structural properties.

Another alternative modelling is the system identification. Modal testings [SM99, Ewi84] have been commonly practised by engineers to determine the modal properties of flexible structures from experiments. This method is only available if the structures concerned are already built. When it is important to integrate the control system on the design stages of structures, it is necessary to use other modelling methods such as approximate methods. System identification will not be discussed here although some issues in relation to optimal placement of actuators and sensors will be discussed briefly in Chapter 5.

Modelling of smart structures is not solely about modelling of ordinary flexible structures. We also have to consider how smart actuators and sensors can be integrated to the structures. Since we concentrate on using piezoelectric transducers, this chapter will also include the modelling of smart structures with piezoelectric actuators and sensors.

2.1 Dynamics of flexible structures

This section discusses the derivations of equations of motion for LTI spatially distributed systems. It is important to understand the limitations of the equations of motion in describing the physical behaviour of systems. An important assumption for the systems is that the deformations of the systems are sufficiently small. In other words, the angle or slope that a structure makes during vibration with respect to its undisturbed position, is relatively small. Thus, a small angle approximation can be employed to simplify the overall derivation by allowing the equations of motion to be linearized. In more complicated systems with multiple components, such as flexible link manipulators or structures with changing configurations, the results from linear vibration analysis can also be used. This is because in many cases, the structural vibration of each component can still be considered small. In this thesis, we will focus on flexural vibration

of smart structures. However, it is also important to mention other types of vibration such as axial and torsional vibrations. The reason is that our results can be readily extended to deal with those types of vibration.

2.1.1 Axial vibration of rods

In smart structures, the axial vibration can be excited by piezoelectric actuators. For example, two piezoelectric patches can be bonded on both sides of the structure. A pure axial deformation can be generated by applying in-phase voltages to both patches as depicted in Figure 2.1 [BSW96].

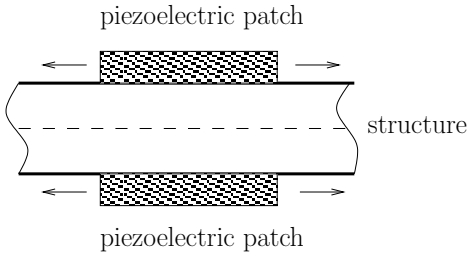

Figure 2.1: Piezoelectric patches for axial vibration

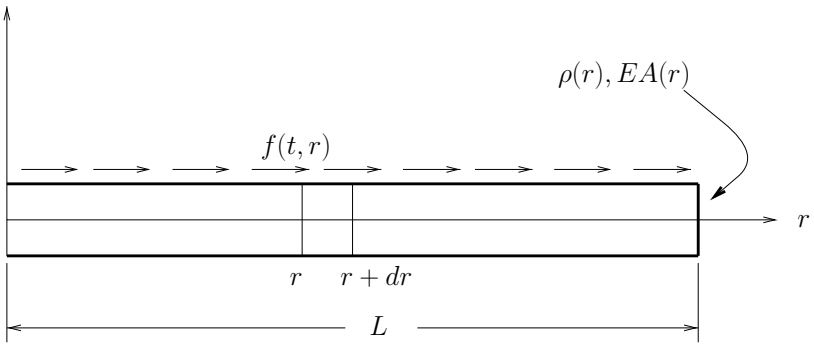

Figure 2.2: A beam in axial vibration

Consider a rod of length L as depicted in Figure 2.2. The distributed axial force, density, cross-sectional area, and Young's modulus of elasticity at point r are defined as f, ρ, A and E respectively. The longitudinal displacement at point r is denoted by u. The main assumptions used are:

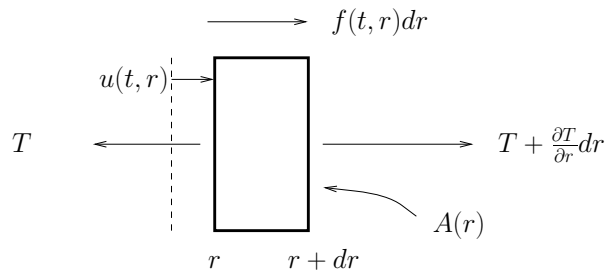

Figure 2.3: A small element of the beam

(i) The material follows Hooke's law , i.e. $\sigma(r) = \epsilon(r)E(r)$, where σ and ϵ are the longitudinal stress and strain at point r respectively [GT91, Pop76, TY68]. This amounts to having a linear relationship between stress and strain.

(ii) The lateral dimensions of the rod are sufficiently smaller than its longitudinal dimension. As a consequence, the radial motion can be neglected.

The free-body diagram of an element dr is shown in Figure 2.3. Applying Newton's second law to the force components in r direction gives

$$\left(T + \frac{\partial T}{\partial r}dr\right) - T + f(t,r)dr = \rho A(r)dr\frac{\partial^2 u(t,r)}{\partial t^2} \tag{2.1}$$

which is equivalent to

$$\frac{\partial T}{\partial r} + f(t,r) = \rho A(r)\frac{\partial^2 u(t,r)}{\partial t^2}. \tag{2.2}$$

From Hooke's law, the tension T is related to the longitudinal strain by

$$T(t,r) \;\; = \;\; EA(r)\frac{\partial u(t,r)}{\partial r} \tag{2.3}$$

where $\partial u/\partial r$ is the longitudinal strain at point r.

Substituting (2.3) into (2.2), the partial differential equation (PDE) that governs the axial vibration of rods is obtained [Mei75, dS00]:

$$\frac{\partial}{\partial r}\left(EA(r)\frac{\partial u(t,r)}{\partial r}\right) + f(t,r) \;\; = \;\; \rho A(r)\frac{\partial^2 u(t,r)}{\partial t^2}, \qquad 0 \le r \le L. \tag{2.4}$$

2.1.2 Torsional vibration of shafts

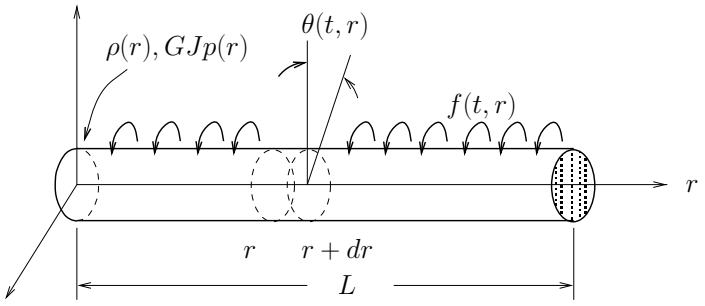

Figure 2.4: A shaft in torsional vibration

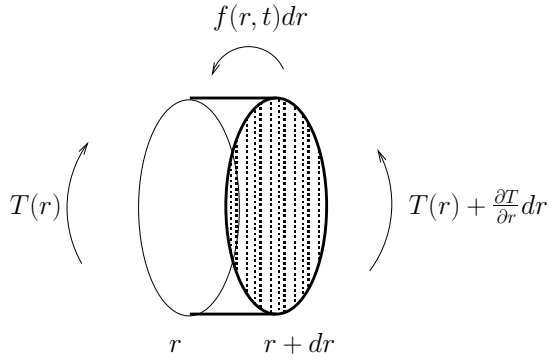

Figure 2.5: A small element of the shaft

Consider a shaft of length L as depicted in Figure 2.4. The density, torque, distributed torque, torsional modulus of elasticity (shear modulus), polar moment of area, and angular displacement at point r are defined as ρ, T, f, G, J_p and θ respectively.

The free-body diagram of an element dr is shown in Figure 2.5. Applying Newton's second law for rotatory motion to torque components in the direction of the r axis gives

$$\left(T + \frac{\partial T}{\partial r}dr\right) - T + f(t,r)dr = \rho J_p(r)dr\frac{\partial^2\theta}{\partial t^2} \tag{2.5}$$

which is equivalent to

$$\frac{\partial T}{\partial r} + f(t,r) = \rho J_p(r)\frac{\partial^2\theta}{\partial t^2}. \tag{2.6}$$

The relationship between the torque and the angular displacement for circular cross sections can be written as [dS00, GT91, Pop76, TY68]:

$$T = GJ_p \frac{\partial \theta}{\partial r} \tag{2.7}$$

where GJ_p is often called the torsional rigidity of the shaft. For the case of a shaft with non-circular cross sections, the polar moment of area J_p in (2.7) must be replaced by the torsional parameter J_t. Some examples for the torsional parameter of non-circular cross sections [dS00, GT91, Pop76, BJ92] are:

- A thin closed section (a thin hollow section):

$$J_t = \frac{4hA_s^2}{p} \tag{2.8}$$

  where A_s is the enclosed area of the hollow section, h is the section thickness, and p is the perimeter of the section.

- A solid square section:

$$J_t = 0.1406d^4 \tag{2.9}$$

  where d is the width (or height) of the square.

- A hollow circular section:

$$J_t = \frac{\pi}{2}\left(r_2^4 - r_1^4\right) \tag{2.10}$$

  where r_1 is the radius of the inner circle and r_2 is the radius of the outer circle.

Substituting (2.7) into (2.6) and re-arranging the equation gives [dS00]

$$\frac{\partial}{\partial r}\left(GJ_p(r)\frac{\partial \theta(t,r)}{\partial r}\right) + f(t,r) = \rho J_p(r)\frac{\partial^2 \theta(t,r)}{\partial t^2}, \quad 0 \le r \le L. \tag{2.11}$$

For a more general case of shafts with non-circular cross sections:

$$\frac{\partial}{\partial r}\left(GJ_t(r)\frac{\partial \theta(t,r)}{\partial r}\right) + f(t,r) = \rho J_p(r)\frac{\partial^2 \theta(t,r)}{\partial t^2}, \quad 0 \le r \le L \tag{2.12}$$

where J_t is the torsional parameter mentioned previously.

2.1.3 Flexural vibration of beams

Flexural vibration can be observed in many structures such as aircraft wings, bridges, buildings and robot manipulators. In some structures, axial and torsional properties may be stiffer than their flexural properties. Hence, minimizing the flexural vibration can be of considerable importance in vibration control of structures. The flexural vibration can be induced by bonding two piezoelectric patches and applying out-of-phase voltages to those patches as depicted in Figure 2.6 [BSW96]. However, it is also sufficient to use a single patch to induce this type of vibration.

The research done in here is concentrated in controlling flexural vibration of structures. However, as mentioned previously, the vibration analysis and control approach discussed in this thesis can also be used for other types of vibrations.

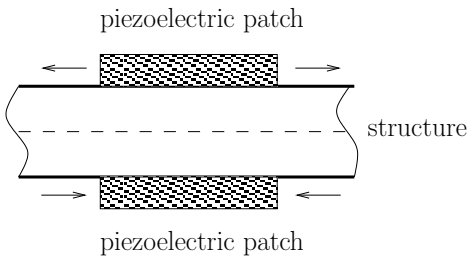

Figure 2.6: Piezoelectric patches for flexural vibration

Consider a thin beam of length L as depicted in Figure 2.7, whose density and flexural rigidity at point r are ρ and EI respectively. The flexural rigidity depends on the Young's modulus of elasticity E and the second moment of area I. The distributed transverse force is f. The main assumptions are:

(i) The material follows Hooke's Law.

(ii) The shear deformation is negligible compared to the bending deformation.

(iii) The rotation of the element is negligible compared to the vertical/transverse translation.

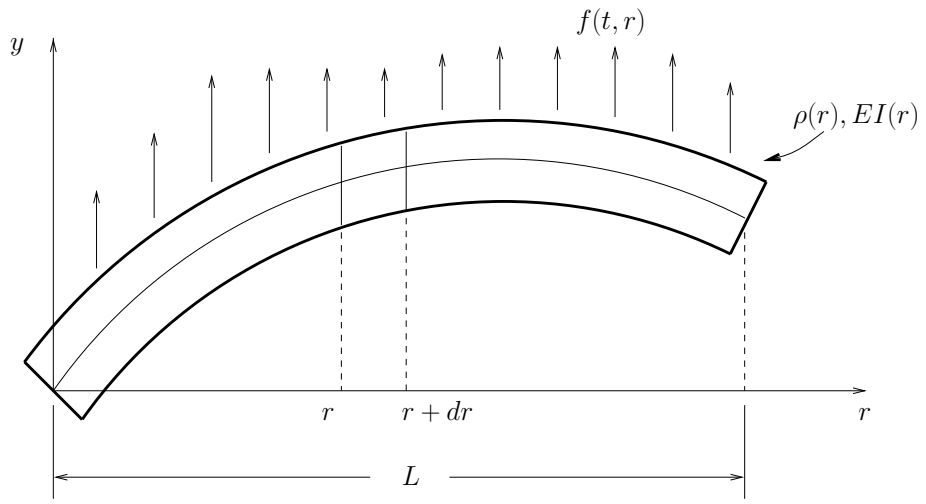

Figure 2.7: A beam in flexural vibration

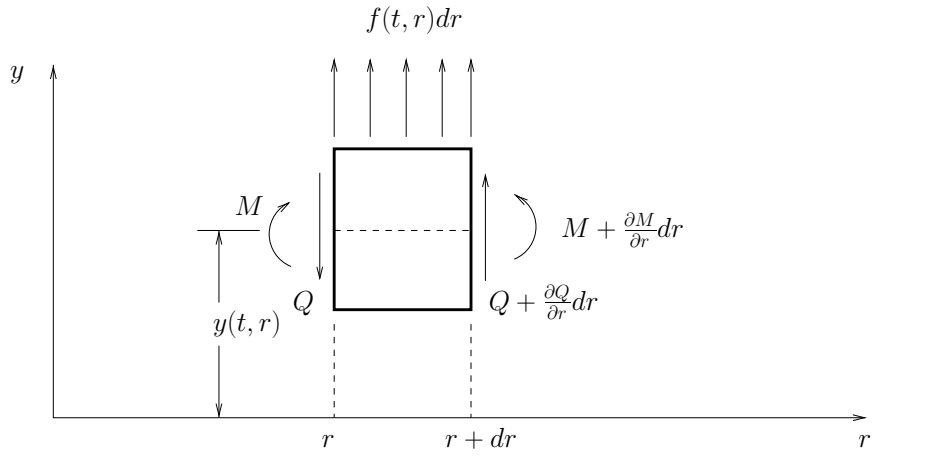

Figure 2.8: A small element of the beam

The free-body diagram of an element dr is shown in Figure 2.8, where Q denotes the shearing force and M the bending moment. Applying Newton's second law to vertical force components (y direction) gives

$$\left(Q(t,r) + \frac{\partial Q(t,r)}{\partial r}dr\right) - Q(t,r) + f(t,r)dr \;=\; \rho A(r)dr\frac{\partial^2 y(t,r)}{\partial t^2} \quad (2.13)$$

which is equivalent to

$$\frac{\partial Q(t,r)}{\partial r} + f(t,r) \;=\; \rho A(r)\frac{\partial^2 y(t,r)}{\partial t^2}. \quad (2.14)$$

Furthermore, considering the moment about the axis normal to r and y (out-of-page direction):

$$\left(M(t,r) + \frac{\partial M(t,r)}{\partial r}dr\right) - M(t,r) + \left(Q(t,r) + \frac{\partial Q(t,r)}{\partial r}dr\right)dr + f(t,r)dr\frac{dr}{2} = 0. \quad (2.15)$$

Simplifying the above equation and cancelling the higher order dr term, the shearing force in terms of the bending moment is

$$Q(t,r) \;=\; -\frac{\partial M(t,r)}{\partial r}. \quad (2.16)$$

Substituting (2.16) into (2.14) gives

$$-\frac{\partial^2 M(t,r)}{\partial r^2} + f(t,r) \;=\; \rho A(r)\frac{\partial^2 y(t,r)}{\partial t^2}. \quad (2.17)$$

The bending moment can be related to the curvature of the element [Mei75, GT91, TY68, Bor62]:

$$M(t,r) \;=\; EI(r)\frac{\partial^2 y(t,r)}{\partial r^2}. \quad (2.18)$$

Substituting this into (2.17) and re-arranging gives

$$\frac{\partial^2}{\partial r^2}\left(EI(r)\frac{\partial^2 y(t,r)}{\partial r^2}\right) + \rho A(r)\frac{\partial^2 y(t,r)}{\partial t^2} = f(t,r), \quad 0 \le r \le L \quad (2.19)$$

which is the Bernoulli-Euler beam equation [Mei75, dS00]. When the beam is relatively thick, the effects of shear deformation and rotational inertia need to be considered. For this type of beam, the Timoshenko beam equation can be used [dS00].

Some common boundary conditions are listed below [Mei75, dS00]:

- Cantilevered (clamped) end at $r = r_o$: The deflection and the slope of the deflection curve are zero.

$$y(t, r_o) = 0, \qquad \left.\frac{\partial y(t,r)}{\partial r}\right|_{r=r_o} = 0. \tag{2.20}$$

- Simply-supported (hinged/pinned) end at $r = r_o$: The deflection and bending moment are zero.

$$y(t, r_o) = 0, \qquad \left. EI(r)\,\frac{\partial^2 y(t,r)}{\partial r^2}\right|_{r=r_o} = 0. \tag{2.21}$$

- Free end at $r = r_o$: The shearing force and bending moment are zero.

$$\left.\frac{\partial}{\partial r}\left(EI(r)\frac{\partial^2 y(t,r)}{\partial r^2}\right)\right|_{r=r_o} = 0, \quad \left. EI(r)\,\frac{\partial^2 y(t,r)}{\partial r^2}\right|_{r=r_o} = 0. \tag{2.22}$$

2.1.4 Flexural vibration of thin plates

The previous flexural beam case assumes a one-dimensional system. In this section, we consider flexural vibration of a two-dimensional structure, a thin plate. We include the derivation of strain and stress in the plate since we intend to use it for modelling piezoelectric laminate plates in Chapter 5. In the same chapter, we will also consider the optimal placement of actuators and sensors over such structures.

Two main assumptions used are:

(i) The plate has a uniform thickness.

(ii) The thin plate assumption: the shear deformation, stress in vertical/transverse direction and rotational inertia of the plate are ignored.

A thin plate with dimensions of $a \times b \times h$ is shown in Figure 2.9. The Young's modulus of elasticity, density and Poisson's ratio of the plate are denoted by E, ρ and ν respectively. Consider the plate element in Figures 2.10 and 2.11. The external moments per unit length are denoted by M_{px} and M_{py}, which may be

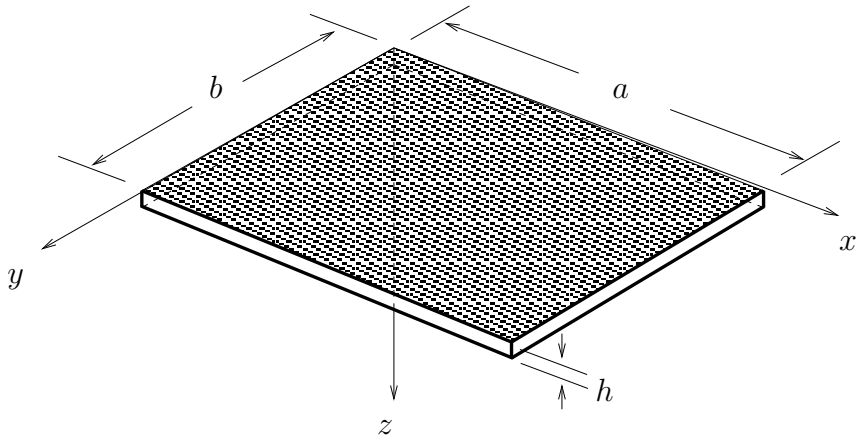

Figure 2.9: A thin plate in flexural vibration

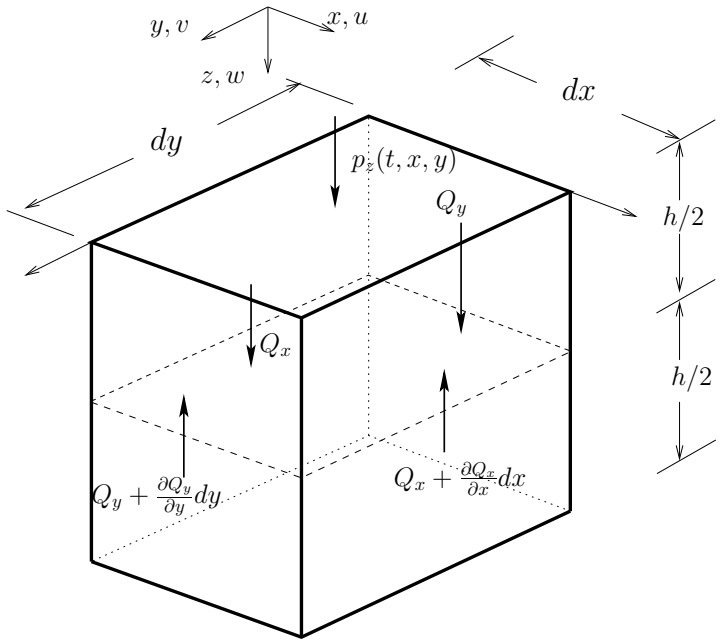

Figure 2.10: A small element of the plate - shear forces

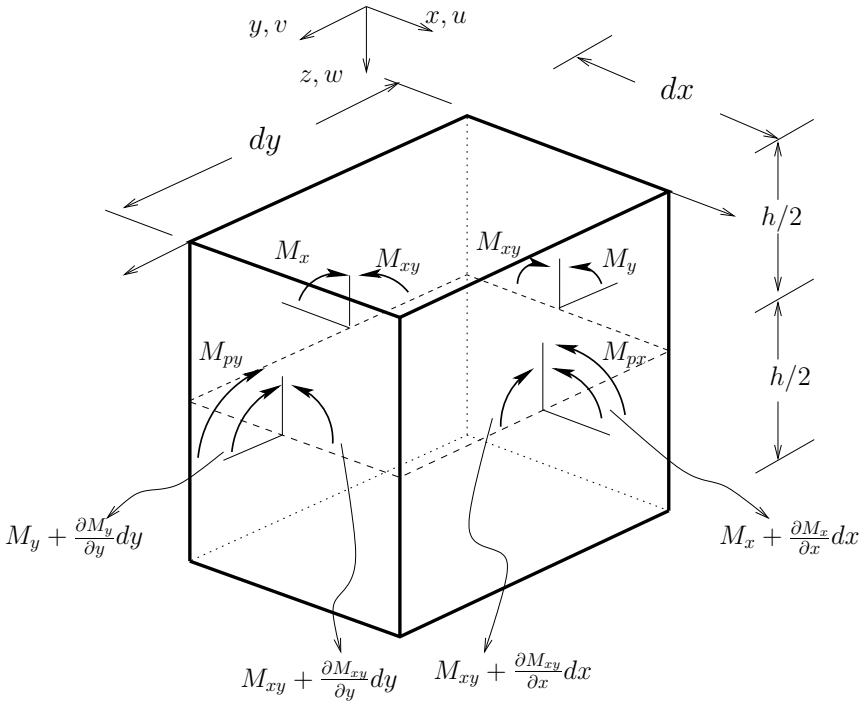

Figure 2.11: A small element of the plate - moments

contributed by piezoelectric actuators. Further, p_z is the pressure in z direction, while Q_x and Q_y are the shearing forces per unit length on planes normal to x and y respectively. The origin of z axis is located on the mid-plane of the plate, i.e. the neutral plane. In pure bending cases, the neutral plane experiences no longitudinal strain or stress. As a consequence, it can be conveniently used as the reference axis for stress-strain calculation purposes. At this point, we concentrate on the plane at a distance z from the neutral plane (mid-plane).

The deflections in x and y directions, u and v, could be expressed as [Jaw94, Man64, Yu96]:

$$\begin{aligned} u &= -z\frac{\partial w}{\partial x} \\ v &= -z\frac{\partial w}{\partial y} \end{aligned} \tag{2.23}$$

where w is the deflection in z direction.

Using Hooke's law [Jaw94, Man64, Yu96], the expression for the strains can be obtained from (2.23):

$$\begin{aligned} \epsilon_x &= \frac{\partial u}{\partial x} = -z\frac{\partial^2 w}{\partial x^2} \\ \epsilon_y &= \frac{\partial v}{\partial y} = -z\frac{\partial^2 w}{\partial y^2} \\ \gamma_{xy} &= \frac{\partial u}{\partial y} + \frac{\partial v}{\partial x} = -2z\frac{\partial^2 w}{\partial x \partial y} \end{aligned} \tag{2.24}$$

where γ_{xy} is the shear strain, while ϵ_x and ϵ_y are the longitudinal strains in x and y directions respectively.

From Hooke's law, strains are related to stresses [Jaw94, Man64, Yu96]:

$$\begin{aligned} \epsilon_x &= \frac{1}{E}(\sigma_x - \nu\sigma_y) \\ \epsilon_y &= \frac{1}{E}(\sigma_y - \nu\sigma_x) \\ \gamma_{xy} &= \frac{1}{G}\tau_{xy} = 2\frac{(1+\nu)}{E}\tau_{xy} \end{aligned} \tag{2.25}$$

where G is the shear modulus and can be related to Young's modulus as described above. Here, τ_{xy} is the shear stress, while σ_x and σ_y are the longitudinal stresses in x and y directions respectively. Hence, the stresses can be determined from (2.24) and (2.25):

$$\begin{aligned} \tau_{xy} &= -\frac{Ez}{(1+\nu)}\frac{\partial^2 w}{\partial x \partial y} \\ \sigma_x &= -\frac{Ez}{(1-\nu^2)}\left(\frac{\partial^2 w}{\partial x^2} + \nu\frac{\partial^2 w}{\partial y^2}\right) \\ \sigma_y &= -\frac{Ez}{(1-\nu^2)}\left(\frac{\partial^2 w}{\partial y^2} + \nu\frac{\partial^2 w}{\partial x^2}\right). \end{aligned} \tag{2.26}$$

The expressions relate stresses with the deflection/curvature of the plate. The next task is to relate bending moments and forces to the stresses so the equations of motion can be obtained.

The moment per unit length M_x is calculated by integrating the corresponding stress across the plate thickness:

$$\begin{aligned} M_x &= \int_{-\frac{h}{2}}^{\frac{h}{2}} z\sigma_x dz \\ &= -D\left(\frac{\partial^2 w}{\partial x^2} + \nu\frac{\partial^2 w}{\partial y^2}\right) \end{aligned} \tag{2.27}$$

where D is often called the flexural rigidity of the plate [Smi88, Yu96]:

$$D = \frac{Eh^3}{12(1-\nu^2)}. \tag{2.28}$$

Similarly for M_y:

$$\begin{aligned} M_y &= \int_{-\frac{h}{2}}^{\frac{h}{2}} z\sigma_y dz \\ &= -D\left(\frac{\partial^2 w}{\partial y^2} + \nu\frac{\partial^2 w}{\partial x^2}\right). \end{aligned} \tag{2.29}$$

The torsional moment per unit length M_{xy} is

$$\begin{aligned} M_{xy} &= \int_{-\frac{h}{2}}^{\frac{h}{2}} z\tau_{xy} dz \\ &= -D(1-\nu)\frac{\partial^2 w}{\partial x \partial y}. \end{aligned} \tag{2.30}$$

Applying Newton's second law to vertical forces (in z direction, see Figure 2.10):

$$\begin{aligned} Q_x dy - \left(Q_x + \frac{\partial Q_x}{\partial x}dx\right)dy + Q_y dx - \left(Q_y + \frac{\partial Q_y}{\partial y}dy\right)dx \\ + p_z(t,x,y)dx\,dy - \rho(x,y)\,h\,dx\,dy\frac{\partial^2 w}{\partial t^2} = 0. \end{aligned} \tag{2.31}$$

Division by $dx\,dy$ yields

$$-\frac{\partial Q_x}{\partial x} - \frac{\partial Q_y}{\partial y} + p_z(t,x,y) - \rho(x,y)h\frac{\partial^2 w}{\partial t^2} = 0. \tag{2.32}$$

Taking moment equilibrium about x axis and ignoring the rotational inertia of the plate (considering shear forces and moments in Figures 2.10 and 2.11):

$$\begin{aligned} p_z(t,x,y)dx\,dy\frac{dy}{2} - \frac{\partial Q_x}{\partial x}dxdy\frac{dy}{2} - \left(Q_y + \frac{\partial Q_y}{\partial y}dy\right)dx\,dy \\ - \frac{\partial M_y}{\partial y}dydx - \frac{\partial M_{xy}}{\partial x}dxdy - M_{py}\,dx = 0. \end{aligned} \tag{2.33}$$

Division by $dx\,dy$ and ignoring the higher order term dy gives

$$-Q_y = \frac{\partial M_y}{\partial y} + \frac{\partial M_{xy}}{\partial x} + \frac{\partial M_{py}}{\partial y}. \tag{2.34}$$

A similar expression can be obtained when the moment equilibrium is taken about y axis:

$$-Q_x = \frac{\partial M_x}{\partial x} + \frac{\partial M_{xy}}{\partial y} + \frac{\partial M_{px}}{\partial x}. \tag{2.35}$$

In this case, $M_{xy} = M_{yx}$ is assumed due to complementary shear stresses $\tau_{xy} = \tau_{yx}$.

We differentiate (2.34) and (2.35) with respect to y and x respectively, and substitute them into the vertical equilibrium equation (2.32):

$$\left(\frac{\partial^2 M_x}{\partial x^2} + 2\frac{\partial^2 M_{xy}}{\partial x \partial y} + \frac{\partial^2 M_y}{\partial y^2}\right) + \left(\frac{\partial^2 M_{px}}{\partial x^2} + \frac{\partial^2 M_{py}}{\partial y^2}\right) + p_z(t,x,y) - \rho(x,y)\, h\frac{\partial^2 w}{\partial t^2} = 0. \quad (2.36)$$

The moments in (2.27), (2.29) and (2.30) can be differentiated twice to obtain $\partial^2 M_x/\partial x^2, \partial^2 M_y/\partial y^2$ and $\partial^2 M_{xy}/\partial x \partial y$. The PDE for the thin uniform plate is obtained after substitution of these equations into (2.36):

$$\rho(x,y)\, h\frac{\partial^2 w}{\partial t^2} + D\nabla^4 w(t,x,y) = \frac{\partial^2 M_{px}}{\partial x^2} + \frac{\partial^2 M_{py}}{\partial y^2} + p_z(t,x,y) \quad (2.37)$$

where

$$\nabla^4 w = \frac{\partial^4 w}{\partial x^4} + 2\frac{\partial^4 w}{\partial x^2 \partial y^2} + \frac{\partial^4 w}{\partial y^4}. \quad (2.38)$$

2.2 Modal analysis

We consider some modelling methods that can be used to solve previous PDE's, starting with the modal analysis method. The method is standard and also can be found in [Mei75, dS00, CSG98]. Consider the typical PDE for spatially distributed systems:

$$\mathcal{L}\{y(t,r)\} + \mathcal{C}\left\{\frac{\partial y(t,r)}{\partial t}\right\} + \mathcal{M}\left\{\frac{\partial^2 y(t,r)}{\partial t^2}\right\} = f(t,r). \quad (2.39)$$

This PDE may describe the axial, torsional and flexural vibrations that we have discussed previously. Here, r is the spatial coordinate, which is defined over a domain $\mathcal{R}$. Also, $\mathcal{L}$ and $\mathcal{M}$ are linear homogeneous differential operators of order $2p$ and $2q$ respectively and $q \leq p$. The general arbitrary input is denoted by f, which is spatially distributed over $\mathcal{R}$.

Furthermore, $\mathcal{C}$ is described as:

$$\mathcal{C} = c_1\mathcal{L} + c_2\mathcal{M} \tag{2.40}$$

where c_1 and c_2 are non-negative constants. This assumes a proportional damping in the system. In practice, it is not easy to model damping accurately, and we may need to rely on experiments. Based on our experimental experience, the proportional damping terms are sufficient to represent damping in flexible structures.

The boundary conditions can be expressed as:

$$\mathcal{B}_\ell \{y(t,r)\} = 0, \qquad \ell = 1, 2, \ldots, p \tag{2.41}$$

where $\mathcal{B}_\ell$ are linear homogeneous differential operators of order up to $2p-1$.

The modal analysis assumes a solution for (2.39) in the form of

$$y(t,r) = \sum_{i=1}^{\infty} \phi_i(r) q_i(t) \tag{2.42}$$

where q_i is the generalized coordinate.

Here, ϕ_i are the eigenfunctions that are obtained by solving the eigenvalue problem associated with (2.39)

$$\mathcal{L}\{\phi_i(r)\} = \lambda_i \mathcal{M}\{\phi_i(r)\}$$

and its associated boundary conditions. This corresponds to the undamped vibration case. The natural frequencies ω_i are determined from the eigenvalues

$$\lambda_i = \omega_i^2, \quad i = 1, 2, \ldots.$$

Since $\mathcal{L}$ is self-adjoint for the majority of systems considered here, the normalized eigenfunctions have the following orthogonality properties:

$$\int_{\mathcal{R}} \phi_i(r)\mathcal{L}\{\phi_j(r)\}dr = \delta_{ij}\omega_i^2 \tag{2.43}$$

$$\int_{\mathcal{R}} \phi_i(r)\mathcal{M}\{\phi_j(r)\}dr = \delta_{ij} \tag{2.44}$$

$$\int_{\mathcal{R}} \phi_i(r)\mathcal{C}\{\phi_j(r)\}dr = 2\delta_{ij}\zeta_i\omega_i \tag{2.45}$$

where δ_{ij} is the Kronecker delta function, where $\delta_{ij} = 1$ for $i = j$, and zero otherwise. The damping factor is then

$$\zeta_i = \frac{c_1\omega_i^2 + c_2}{2\omega_i}. \tag{2.46}$$

Substituting (2.42) in (2.39), we obtain

$$\mathcal{L}\left\{\sum_{i=1}^{\infty}\phi_i(r)q_i(t)\right\} + \mathcal{C}\left\{\frac{\partial}{\partial t}\sum_{i=1}^{\infty}\phi_i(r)q_i(t)\right\} + \mathcal{M}\left\{\frac{\partial^2}{\partial t^2}\sum_{i=1}^{\infty}\phi_i(r)q_i(t)\right\} = f(t,r). \tag{2.47}$$

The orthogonality of the eigenfunctions allows the PDE to be transformed into a set of ordinary differential equations (ODE's). Multiplying (2.47) by ϕ_j and integrating over the domain $\mathcal{R}$, taking advantage of the orthogonality conditions (2.43), (2.44) and (2.45), we obtain

$$\ddot{q}_i(t) + 2\zeta_i\omega_i\dot{q}_i(t) + \omega_i^2 q_i(t) = Q_i(t), \qquad i = 1, 2, \ldots \tag{2.48}$$

where the generalized force is

$$Q_i(t) = \int_{\mathcal{R}} \phi_i(r) f(t,r) dr. \tag{2.49}$$

In control design, a frequency domain model is often required. To obtain the model in frequency domain, the above equations can be solved by Laplace transforms. The generalized force is related to the system input u as

$$Q_i(t) = P_i u(t) \tag{2.50}$$

where P_i is the time-independent forcing term.

Then, the transfer function of the system can be shown to be

$$G(s,r) = \sum_{i=1}^{\infty} \frac{\phi_i(r)P_i}{s^2 + 2\zeta_i\omega_i s + \omega_i^2}. \tag{2.51}$$

In the following, we will discuss the modal analysis solution for simply-supported beams and simply-supported thin plates that will be used in some parts of the thesis.

2.2.1 Simply-supported beams

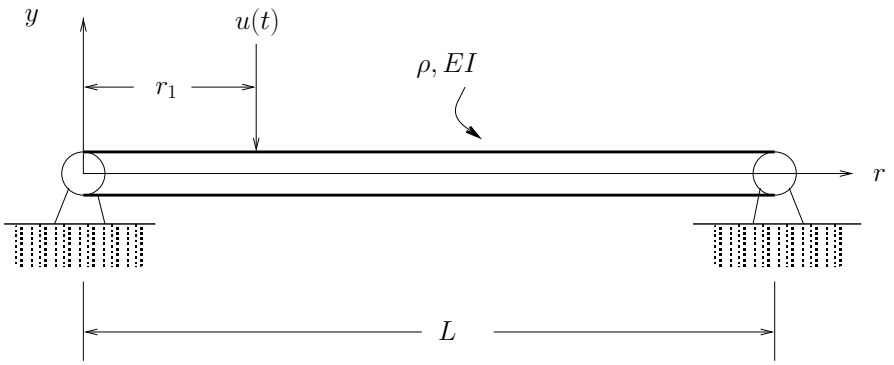

Figure 2.12: A simply-supported beam

Consider a simply-supported uniform beam of length L where a point force u is acting at point $r = r_1$ as depicted in Figure 2.12. The solution for a point force here can provide information for systems with general excitation since the systems are linear. The PDE that governs the beam is (2.19) and the boundary conditions are as described in (2.21):

$$\begin{aligned} y(t,0) &= 0 \\ y(t,L) &= 0 \\ EI\left.\frac{\partial^2 y(t,r)}{\partial r^2}\right|_{r=0} &= 0 \\ EI\left.\frac{\partial^2 y(t,r)}{\partial r^2}\right|_{r=L} &= 0. \end{aligned} \tag{2.52}$$

Considering the general notations in (2.39) and (2.41):

$$\begin{aligned} \mathcal{L} &= \frac{\partial^2}{\partial r^2}\left(EI\frac{\partial^2}{\partial r^2}\right) \\ \mathcal{M} &= \rho A \\ \mathcal{B}_1 &= 1 \\ \mathcal{B}_2 &= EI\frac{\partial^2}{\partial r^2} \\ f(t,r) &= u(t)\delta(r-r_1) \end{aligned} \tag{2.53}$$

and $\mathcal{R} = [0, L]$. Further, $\mathcal{C}$ is defined as in (2.40) to include the effect of damping

in the structure. The orthogonality conditions can be written as:

$$\int_0^L \phi_i(r)\phi_j(r)\rho A dr = \delta_{ij} \tag{2.54}$$

$$\int_0^L \phi_i(r)\phi_j''''(r)EI dr = \omega_i^2\delta_{ij} \tag{2.55}$$

where ω_i and ϕ_i are the solutions to the eigenvalue problem

$$\phi_i''''(r) - \lambda_i^4\phi_i(r) = 0 \tag{2.56}$$

and

$$\lambda_i^4 = \frac{\rho A\omega_i^2}{EI}. \tag{2.57}$$

The eigenfunctions ϕ_i have to satisfy the corresponding boundary conditions in (2.52):

$$\begin{aligned} \phi_i(0) &= 0 \\ \phi_i(L) &= 0 \\ \phi_i''(0) &= 0 \\ \phi_i''(L) &= 0. \end{aligned} \tag{2.58}$$

The general solution to the eigenvalue problem is of the form [Mei75, dS00]

$$\phi_i(r) = A_i \sin\lambda_i r + B_i \cos\lambda_i r + C_i \sinh\lambda_i r + D_i \cosh\lambda_i r. \tag{2.59}$$

The first and third boundary conditions in (2.58) imply $B_i = D_i = 0$. The remainder of the boundary conditions imply that $C_i = 0$ and $\sin\lambda_i L = 0$, where

$$\lambda_i = \frac{i\pi}{L}, \quad i = 1, 2, \ldots \tag{2.60}$$

Thus, ϕ_i can be written as $\phi_i = A_i \sin\lambda_i r$. Substituting this expression into the orthogonality condition, the expression for A_i can be found as $A_i = \sqrt{\frac{2}{\rho AL}}$. To summarize, for the simply-supported beam in Figure 2.12, the eigenfunctions are given by sinusoidal functions

$$\phi_i(r) = \sqrt{\frac{2}{\rho AL}} \sin\left(\frac{i\pi r}{L}\right), \quad i = 1, 2, \ldots \tag{2.61}$$

and the corresponding natural frequencies are

$$\omega_i = \left(\frac{i\pi}{L}\right)^2 \sqrt{\frac{EI}{\rho A}}, \quad i = 1, 2, \ldots \tag{2.62}$$

We introduce damping into the system, where ζ_i denotes the damping ratio associated with mode i. Then, the transfer function from the applied force $u(s)$ to the transverse deflection of the beam $y(s, r)$ is found to be:

$$\frac{y(s,r)}{u(s)} = \sum_{i=1}^{\infty} \frac{\phi_i(r_1)\phi_i(r)}{s^2 + 2\zeta_i\omega_i s + \omega_i^2}. \tag{2.63}$$

2.2.2 Simply-supported rectangular thin plates

Consider a rectangular uniform thin plate whose edges are simply-supported. The boundary conditions are:

$$\begin{aligned} w(t,x,y) = 0, M_x &= -D\left(\frac{\partial^2 w}{\partial x^2} + \nu\frac{\partial^2 w}{\partial y^2}\right) = 0, \ \forall x = 0, a; \ 0 \le y \le b \\ w(t,x,y) = 0, M_y &= -D\left(\frac{\partial^2 w}{\partial y^2} + \nu\frac{\partial^2 w}{\partial x^2}\right) = 0, \ \forall y = 0, b; \ 0 \le x \le a. \end{aligned} \tag{2.64}$$

The procedure is similar to that of the beam, so it is not repeated here. The difference is that the eigenfunctions are now functions of x and y. It can be shown that the normalized eigenfunction associated with mode (m, n), where m and n are the mode numbers in x and y directions respectively, is [dS00]

$$\phi_{mn}(x,y) = \frac{2}{\sqrt{ab\rho h}} \sin\frac{m\pi x}{a} \sin\frac{n\pi y}{b}. \tag{2.65}$$

The natural frequency of mode (m, n) is

$$\omega_{mn} = \pi^2 \sqrt{\frac{D}{\rho h}} \left(\frac{m^2}{a^2} + \frac{n^2}{b^2}\right). \tag{2.66}$$

Typical simply-supported mode shapes of a plate are shown in Figure 2.13.

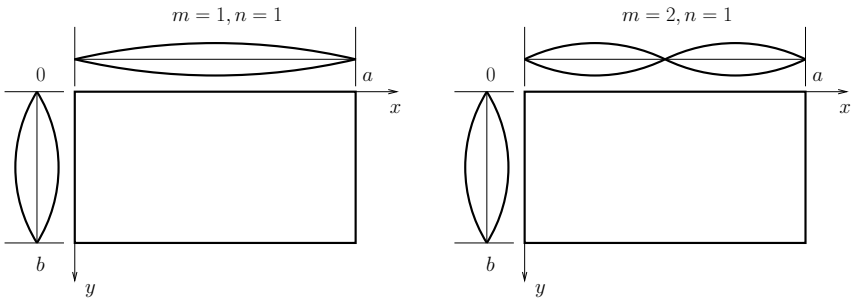

(a) Mode $(1, 1)$ (b) Mode $(2, 1)$

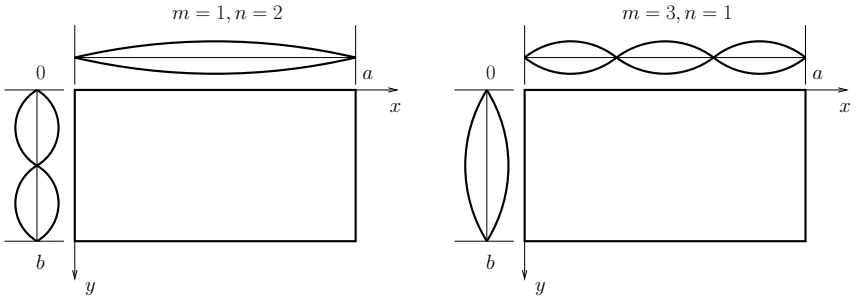

(c) Mode $(1, 2)$ (d) mode $(3, 1)$

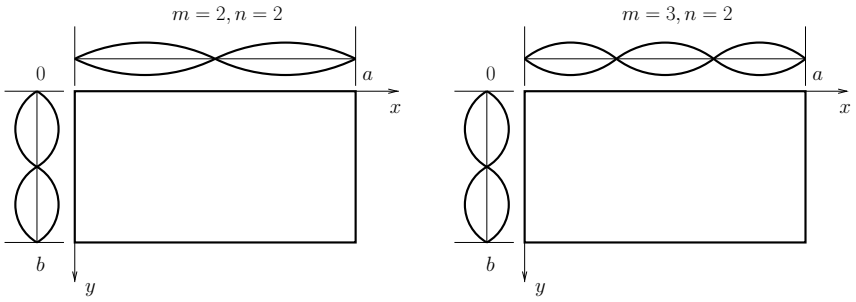

(e) Mode $(2, 2)$ (f) Mode $(3, 2)$

Figure 2.13: Mode shapes of a simply-supported plate

2.3 Rayleigh-Ritz method

We can use the above modal analysis procedure to model systems with uniform properties and relatively simple boundary conditions. However, the approximate solutions are required when the systems have non-uniform properties or the boundary conditions are complicated. In fact, when smart materials are bonded to a structure, the system properties are no longer uniform due to changes in stiffness and mass properties. This can be important when the contribution of smart materials to the structural mass and stiffness properties are considerable. Several methods can be used to model such systems, the Rayleigh-Ritz method being one.

The Rayleigh-Ritz method is an extension of the Rayleigh's energy method that is used to determine the upper bound of the fundamental resonance frequency of a system. The method is based on the Rayleigh's principle which states that the Rayleigh's quotient is stationary in the neighbourhood of the natural mode [Mei75]. The Rayleigh's quotient R can be defined as:

$$\omega^2 = R = \frac{\mathcal{V}_{max}}{\mathcal{T}^*}. \tag{2.67}$$

Here, $\mathcal{V}_{max}$ and $\mathcal{T}^*$ are the maximum potential energy and the reference kinetic energy respectively.

The method assumes the solution as a linear combination of a finite number N of linearly independent admissible functions ϕ_i. The admissible functions only need to satisfy the geometric boundary conditions of the system. The solution is in the form of

$$y(r) = \sum_{i=1}^{N} \phi_i(r) a_i \tag{2.68}$$

where coefficients a_i are to be determined such that the Rayleigh's quotient is stationary. Here, ϕ_i are also called trial functions.

In this case, only admissible functions are required since the natural boundary conditions are included in the potential and kinetic energy. The functions to be chosen have to be differentiable to the order of the associated differential

equation. The solutions yield the upper bounds of the exact natural frequencies since the model is restricted to have only a finite number of discrete systems. The more we have admissible functions used as trial functions, the closer the upper bounds will be to the exact natural frequencies.

2.4 Assumed-modes method

Another approximate method for modelling flexible structures is the assumed-modes method. The method also depends on the combinations of N admissible (trial) functions ϕ_i but with time-dependent coefficients b_i in the form of

$$y(t,r) = \sum_{i=1}^{N} \phi_i(r) b_i(t). \tag{2.69}$$

The method incorporates Lagrange's equation of motion to determine the time-dependent coefficients. Since this method considers the time-dependent response explicitly, it is convenient in dealing with systems with external forces and initial excitation [Mei75].

The assumed-modes method yields the same eigenvalue problem as the Rayleigh-Ritz method when the Rayleigh's quotient is expressed in energies [Mei75]. Both methods are useful when eigenfunctions satisfying the eigenvalue problem and boundary conditions do not exist. However, the accuracy of the solutions depend greatly on the choice of the admissible functions and the number of trial functions used.

2.5 Finite element method

The Rayleigh-Ritz and assumed-modes methods require an appropriate choice of trial functions. However, selecting appropriate trial functions may be difficult for complicated structures.

The FE method can be used for modelling general flexible structures with non-uniform properties and complicated boundary conditions. In addition, experimental modal analysis can be integrated with the FE model to obtain a

realistic model of a system [Ewi84, Fri95]. The disadvantage of the method is that to obtain a sufficiently accurate model it may require a large number of elements, although a model reduction can be done later on. An example of modelling of piezoelectric laminate beam using the FE method will be discussed in Section 2.7.

2.6 Modal analysis modelling of piezoelectric laminate structures

In this section, we consider the modelling of piezoelectric laminate structures. In particular, we will deal with the case of flexural vibration of piezoelectric laminate beams.

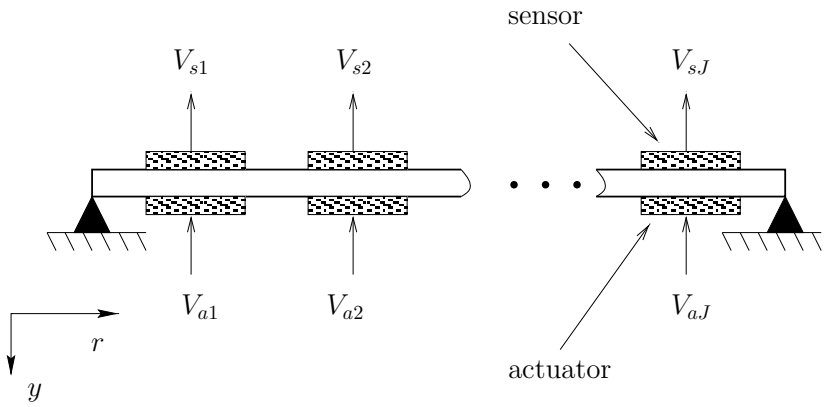

Figure 2.14: A beam with collocated piezoelectric actuators and sensors

Consider a homogeneous Euler-Bernoulli beam with a number of piezoelectric actuator/sensor pairs attached to it (i.e. a piezoelectric laminate beam) as shown in Figure 2.14. Suppose there are J actuators distributed along the structure. Suppose that the j^{th} piezoelectric actuator has dimensions of $L_{pj} \times W_{pj} \times h_{pj}$, where h_{pj} is the thickness of each patch, while the beam has dimensions of $L \times W \times h$ (see Figure 2.15). The applied voltages to the actuating patches are denoted by $V_a = [V_{a1} \dots V_{aJ}]^T$.

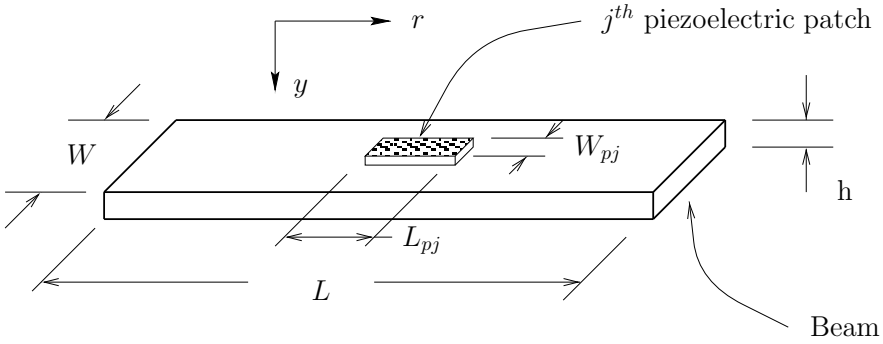

Figure 2.15: A beam with the j^{th} piezoelectric patch attached

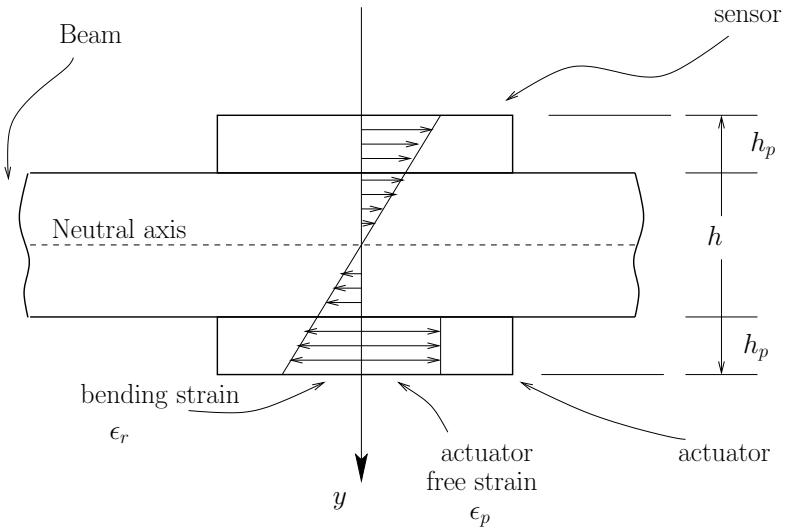

Figure 2.16: The strain distribution of a beam section

The PDE for flexural vibrations of a beam is as in (2.19), assuming a uniform beam:

$$EI\,\frac{\partial^4 y(t,r)}{\partial r^4} + \rho A \frac{\partial^2 y(t,r)}{\partial t^2} \quad = \quad \frac{\partial^2 M_{pr}(t,r)}{\partial r^2} \tag{2.70}$$

where the parameters are as defined in Section 2.1. The right-hand-side of the equation represents the bending moment contribution by piezoelectric actuators. It is assumed that the mass and stiffness contributions of the patches are considerably smaller than those of the beam so they can be ignored. This is true for the piezoelectric patches that are used in our experiments. This simplifies the solution for the beam dynamics since a uniform beam can be considered. Based on our experiments, this uniform beam assumption works sufficiently well for the structures used in the experiments.

The approach presented below follows the procedures in [DFR91, FEN96]. Consider the j^{th} piezoelectric actuator attached to the beam. Let us drop the subscript j for the time being, realizing that the properties that we are about to discuss belong to the j^{th} actuator. The overall longitudinal strain inside the actuator is contributed by the induced longitudinal strain due to bending ϵ_r and the free strain ϵ_p. The free/unconstrained strain is the strain that is generated in the patch due to the applied voltage only [DFR91, FEN96]. An expression for the free strain (see Figure 2.16) of the piezoelectric material is [FEN96, BSW96]

$$\epsilon_p = \left(\frac{d_{31}}{h_p}\right) V_{aj}(t). \tag{2.71}$$

The piezoelectric charge constant d_{31} relates how much mechanical strain is generated when a particular voltage V_{aj} is applied across the piezoelectric patch. The strain distribution is assumed to be uniform across the patch. We ignore the equilibrium conditions that require the strain at the patch boundary to be zero, since the patch is thin relative to its length (see [DFR91]). Moreover, it is assumed that the piezoelectric patches are used at room temperature and the variation of properties with temperature is negligible. Using Hooke's law to

obtain an expression for stress in terms of strain:

$$\begin{aligned} \sigma_{pr} &= E_p\,(\epsilon_r - \epsilon_p) \\ \sigma_r &= E\epsilon_r \end{aligned} \tag{2.72}$$

where σ_{pr} and σ_r are the longitudinal stresses of the actuator and the beam respectively, in r direction, and E_p is the Young's modulus of elasticity of the actuator.

The strain distribution across the beam thickness can be considered to be linear for pure flexural case $\epsilon_r = \alpha\, y$ as shown in Figure 2.16. The strain gradient α is determined from the moment equilibrium equation about the neutral axis of the beam:

$$\int_{-\frac{h}{2}}^{\frac{h}{2}} y\,\sigma_r\,dy + \int_{\frac{h}{2}}^{\frac{h}{2}+h_p} y\,\sigma_{pr}\,dy = 0. \tag{2.73}$$

where the neutral axis is the axis in which the beam longitudinal strain and stress are zero for pure flexural case. It is assumed that the piezoelectric patch is bonded to the beam perfectly. This amounts to having no shearing effect in the patch-structure interface. The assumption of thin patches also implies that the position of the neutral axis does not change with the addition of patches.

The moment equilibrium implies that the bending moment generated by the patch is directly transferred to the structure. From (2.72) and (2.73), the free actuator strain ϵ_p can be expressed and the bending strain gradient α is

$$\alpha = \kappa\,\epsilon_p \tag{2.74}$$

where

$$\kappa = \frac{12\,E_p\,h_p\,(h_p + h)}{2\,E\,h^3 + E_p\,[(h + 2\,h_p)^3 - h^3]}. \tag{2.75}$$

Suppose that the ends of the j^{th} piezoelectric patch are located at r_{1j} and r_{2j} along r axis. Step functions $H(\cdot)$ are used to represent the placement of the patch over the structure. The bending moment experienced by the beam M_{prj} can be determined using (2.74) and the first integral term in (2.73):

$$M_{prj} = K_j\,[H(r - r_{1j}) - H(r - r_{2j})]\,V_{aj}(t) \tag{2.76}$$

where

$$K_j = \frac{\kappa_j E d_{31j} h^3 W_{pj}}{12 h_{pj}} \tag{2.77}$$

which depends on the properties of the beam and the j^{th} piezoelectric patch. Here, $H(r - r_{1j})$ is zero for $r < r_{1j}$ and one for $r \geq r_{1j}$. The forcing term in the PDE (2.70) can then be determined from the M_{prj} expression, using the property of Dirac delta function [KS91]:

$$\int_{-\infty}^{\infty} \delta^{(n)}(t-\theta)\,\phi(t)\,dt = (-1)^n\,\phi^{(n)}(\theta) \tag{2.78}$$

where $\delta^{(n)}$ is the n^{th} derivative of δ and ϕ is continuous at θ.

The modal analysis technique is used to solve the PDE (2.70) by assuming a solution in the form of

$$y(t,r) = \sum_{i=1}^{\infty} \phi_i(r)\,q_i(t). \tag{2.79}$$

Using the orthogonality properties of ϕ_i and Dirac delta function property (2.78), the generalized force can be found as in (2.49):

$$\begin{aligned} Q_{ij} &= \int_0^L \phi_i(r) \frac{\partial^2 M_{prj}}{\partial r^2} dr \\ &= K_j \Psi_{ij}\, V_{aj}(t) \end{aligned} \tag{2.80}$$

where

$$\begin{aligned} \Psi_{ij} &= \int_0^L \phi_i(r) \left[\frac{d\delta(r-r_{1j})}{dr} - \frac{d\delta(r-r_{2j})}{dr} \right] dr \\ &= \frac{d\phi_i(r_{2j})}{dr} - \frac{d\phi_i(r_{1j})}{dr}. \end{aligned} \tag{2.81}$$

Then, by considering the bending moments generated by all J piezoelectric actuators, the following decoupled second-order ODE's are obtained:

$$\ddot{q}_i(t) + 2\zeta_i\,\omega_i\,\dot{q}_i(t) + \omega_i^2\,q_i(t) = \sum_{j=1}^{J} K_j \Psi_{ij}\,V_{aj}(t) \tag{2.82}$$

where $i = 1, 2, \cdots$ and the subscript j denotes the j^{th} actuator.

Applying the Laplace transform to (2.82), assuming zero initial conditions, the MIIO (Multiple-Input, Infinite-Output) transfer function from the applied actuator voltage $V_a(s) = [V_{a1}(s) \dots \ V_{aJ}(s)]^T$ to the beam deflection $y(s,r)$ is

$$G(s,r) \ = \ \sum_{i=1}^{\infty} \frac{\phi_i(r)\, P_i}{s^2 \ + 2\zeta_i\, \omega_i\, s + \omega_i^2} \tag{2.83}$$

where

$$P_i = [K_1 \Psi_{i1} \dots K_J \Psi_{iJ}]. \tag{2.84}$$

2.6.1 Piezoelectric sensors

Suppose J piezoelectric sensors are placed on a structure. Consider the k^{th} piezoelectric sensor patch attached to the beam. All properties described in the following paragraphs belong to the k^{th} piezoelectric patch. It is assumed that the piezoelectric sensor is placed on the beam as shown in Figure 2.16.

When the beam experiences structural deformations, the piezoelectric sensors generate electric charges due to piezoelectric effect. The electric charge distribution q_p, i.e. the charge per unit length, for a one-dimensional structure is [PA95]

$$q_p(t) = \frac{k_{31}^2}{g_{31}}\, W_p\, \epsilon_r \tag{2.85}$$

where k_{31} is the electromechanical coupling factor and g_{31} is the piezoelectric voltage constant in r direction. Since the sensor is placed on the surface of the structure as shown in Figure 2.16, the sensor strain is

$$\epsilon_r = -y_p \frac{\partial^2 y}{\partial r^2} \tag{2.86}$$

where $y_p = -\frac{h+h_p}{2}$ is the normal distance from the neutral axis to the mid-plane of the sensor patch.

The overall electric charge generated can be obtained by integrating the charge q_p (2.85) over the length of the sensor. Substituting the modal analysis solution form (2.79), the induced sensor voltage V_{sk} for the k^{th} sensor is

$$V_{sk}(t) \ = \ \Omega_k \sum_{i=1}^{\infty} \int_{r_{1k}}^{r_{2k}} \frac{d^2\phi_i(r)}{dr^2}\, dr\, q_i(t) \tag{2.87}$$

where

$$\Omega_k = \frac{W_{pk}\, k_{31k}^2}{C_k\, g_{31k}} \left(\frac{h + h_{pk}}{2} \right) \tag{2.88}$$

and C_k is the capacitance of the piezoelectric sensor. The integral given in the above equation can be shown to be equal to Ψ_{ij} in (2.81) when j is replaced by k. So the contribution of each mode to the overall sensor voltage is proportional to Ψ_{ik}.

Taking the Laplace transform of (2.82) and (2.87), the MIMO (Multiple-Input, Multiple-Output) transfer function from the actuator voltage $V_a(s)$ to the sensor voltage $V_s(s) = [V_{s1}(s) \dots V_{sJ}(s)]^T$ is

$$G_{Vs}(s) \;=\; \sum_{i=1}^{\infty} \frac{\Upsilon_i P_i}{s^2 \, + 2\zeta_i\, \omega_i\, s + \omega_i^2} \tag{2.89}$$

where $\Upsilon_i = [\Omega_1 \Psi_{i1} \dots \Omega_J \Psi_{iJ}]^T$. For certain cases such as when actuators and sensors are compatible and collocated, then $\Upsilon_i P_i$ is a positive or negative semi-definite matrix, depending on the polarity of each sensor with respect to its collocated actuator. This collocated nature leads to a minimum phase property for flexible structure systems that has desirable implications on control design. This issue will be discussed further in Chapter 6.

Similar transfer functions can be obtained for more complicated structures, such as plates with certain boundary conditions and tubular structures, by using approximate methods such as the FE method. The modelling of piezoelectric laminate beam via FE method will be discussed next.

2.7 Finite element modelling of piezoelectric laminate structures

When a flexible structure to be modelled is complicated, it is usually not possible to use modal analysis for modelling. Alternatively, approximate methods can be used for modelling such a structure. However, the approximate methods such as the Rayleigh-Ritz and assumed-modes methods rely on the choice of the

admissible functions. The model obtained may not be accurate if the functions chosen are far away from the actual eigenfunctions. The choice of the functions will be more difficult if the structure is complicated.

Finite element method also relies on the admissible functions, but they are defined on each element instead. The method divides a complex system into a finite number of simpler sub-systems. The information of the system is contained in grid points or nodes. This section will discuss the finite element formulation of a flexible beam with piezoelectric actuators and sensors attached to it. We consider the flexural vibration of beams described in the previous section.

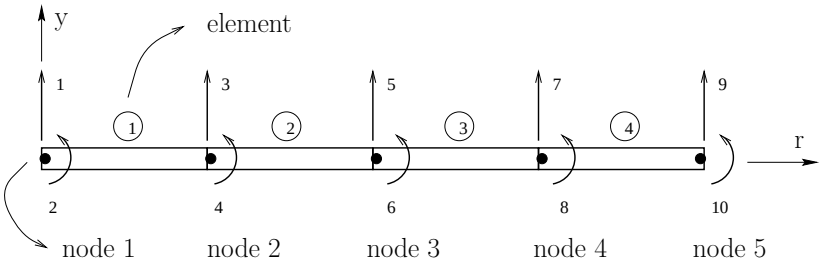

Figure 2.17: A finite element beam

A model of a FE beam of length L with four elements is shown in Figure 2.17. A complicated structure can be divided into simpler elements. Here, we consider the case in which each element can be regarded as a homogeneous beam element. It can be shown that the solution to FE converges to the solution of the associated PDE by increasing the number of elements [Mei75]. Because the FE method used here is standard, only some essential formulations will be discussed in this section. More detailed descriptions can be found in [Mei75, CB97, OP92, Ros91].

Consider a uniform elemental beam of length h_e shown in Figure 2.18. The global axis is denoted by r, while the local (elemental) axis is denoted by r_e. The Young's Modulus E, moment of inertia I, density ρ_b, and cross-sectional area A_b of the element are constants. Each elemental beam has four degrees of freedom, two transverse displacements and two angular displacements as shown

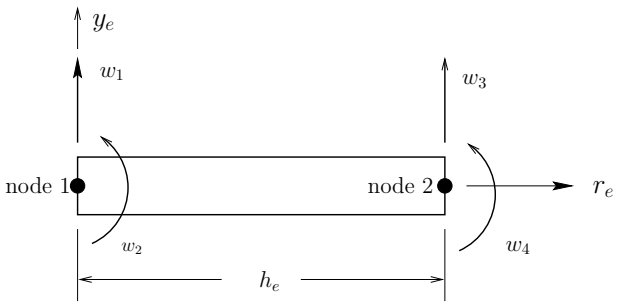

Figure 2.18: An elemental beam

in Figure 2.18. The nodal displacements of the elemental beam can be written as $w_e = [w_1 \quad w_2 \quad w_3 \quad w_4]^T$. The location of a particular point on this elemental beam is denoted by r_e.

The FE method discretizes a continuous system whose structural information is contained in the nodes. Hence, the information between nodes need to be estimated using admissible functions which are also called the shape functions. The shape functions commonly used for this flexural beam case are the Hermite cubic polynomials:

$$\bar{H}(r_e) = \begin{bmatrix} \bar{H}_1 & \bar{H}_2 & \bar{H}_3 & \bar{H}_4 \end{bmatrix}^T \tag{2.90}$$

where

$$\begin{aligned} \bar{H}_1(r_e) &= 1 - 3\left(\frac{r_e}{h_e}\right)^2 + 2\left(\frac{r_e}{h_e}\right)^3 \\ \bar{H}_2(r_e) &= h_e\left[\left(\frac{r_e}{h_e}\right) - 2\left(\frac{r_e}{h_e}\right)^2 + \left(\frac{r_e}{h_e}\right)^3\right] \\ \bar{H}_3(r_e) &= 3\left(\frac{r_e}{h_e}\right)^2 - 2\left(\frac{r_e}{h_e}\right)^3 \\ \bar{H}_4(r_e) &= h_e\left[-\left(\frac{r_e}{h_e}\right)^2 + \left(\frac{r_e}{h_e}\right)^3\right]. \end{aligned} \tag{2.91}$$

Thus, the transverse displacement at any point along the beam w_e can be approximated by

$$w_e(t, r_e) = \bar{H}(r_e)^T w_e(t). \tag{2.92}$$

The elemental mass matrix M_e can be obtained by considering the kinetic energy of the beam element:

$$\begin{aligned}\mathcal{T}_e &= \frac{1}{2}\int_0^{h_e} \rho_b A_b \left(\frac{\partial w_e(t,r_e)}{\partial t}\right)^2 dr_e \\ &= \frac{1}{2}\int_0^{h_e} \rho_b A_b\, \dot{w}_e(t)^T\, \bar{H}(r_e)\bar{H}(r_e)^T\, \dot{w}_e(t) dr_e \\ &= \frac{1}{2}\,\dot{w}_e(t)^T\, M_e\, \dot{w}_e(t) \end{aligned} \tag{2.93}$$

where $M_e = \rho_b A_b \int_0^{h_e} \bar{H}(r_e)\bar{H}(r_e)^T\, dr_e$.

The elemental stiffness matrix K_e can be obtained in a similar way. The strain energy of the beam $\mathcal{V}_e$ can be obtained from

$$\begin{aligned}\mathcal{V}_e &= \frac{1}{2}\int_0^{h} EI \left(\frac{\partial^2 w_e(t,r_e)}{\partial r_e^2}\right)^2 dr_e \\ &= \frac{1}{2}\int_0^{h_e} EI\, w_e(t)^T \left(\frac{d^2\bar{H}(r_e)}{dr_e^2}\right)\left(\frac{d^2\bar{H}(r_e)}{dr_e^2}\right)^T w_e(t) dr_e \\ &= \frac{1}{2}\, w_e(t)^T\, K_e\, w_e(t) \end{aligned} \tag{2.94}$$

where $K_e = EI \int_0^{h_e} \left(\frac{d^2\bar{H}(r_e)}{dr_e^2}\right)\left(\frac{d^2\bar{H}(r_e)}{dr_e^2}\right)^T dr_e$.

Suppose N elements are used to model the beam and k is the number of degrees of freedom of the beam. We introduce the subscript n to denote the properties of the n^{th} elemental beam. The n^{th} elemental nodal displacements w_{e_n} are expressed in terms of the global displacements w by using a linear transformation matrix A_n:

$$w_{e_n}(t) = A_n\, w(t) \tag{2.95}$$

where $w_{e_n} \in \mathbf{R}^{4\times 1}, w \in \mathbf{R}^{k\times 1}$ and $A_n \in \mathbf{R}^{4\times k}$.

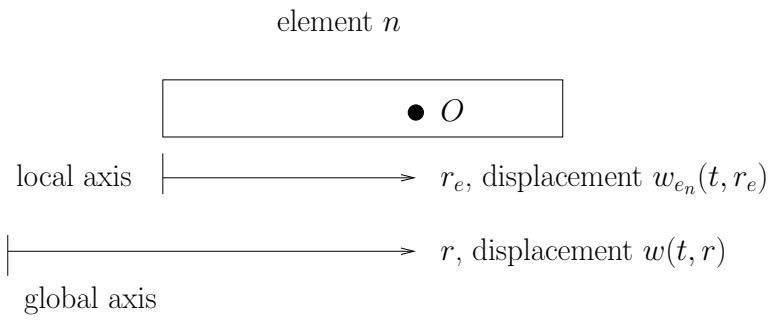

Figure 2.19: The axes system

The transverse deflection of the beam w at a particular location r can be determined from the displacement of the corresponding elemental beam at distance r_e. Here, $r \in \mathcal{R} = \{r \mid 0 \leq r \leq L\}$ and $r_e \in \mathcal{R}_1 = \{r_e \mid 0 \leq r_e \leq h_e\}$. For instance, the point O in Figure 2.19 is located at r in the n^{th} elemental beam. The corresponding local coordinate for the elemental beam is r_e. The transverse deflection w of point O can be obtained only from the nodal displacements of the n^{th} elemental beam, w_{e_n}.

The global displacement w can be determined using (2.92) and (2.95):

$$\begin{aligned} w(t,r) &= w_{e_n}(t,r_e) = \bar{H}(r_e)^T\, w_{e_n}(t) \\ &= \bar{H}(r_e)^T\, A_n\, w(t) \\ &= C_w(r)\, w(t) \end{aligned} \tag{2.96}$$

where $C_w(r) = \bar{H}(r_e)^T\, A_n \in \mathbf{R}^{1\times k}$.

2.7.1 Global nodal force vector, $\hat{F}$

The global force vector describes all external forces applied to the overall structure. The global nodal force vector due to piezoelectric actuators can be obtained by calculating the virtual work done by the beam. The distributed forces are represented as the equivalent nodal forces. Consider the j^{th} piezoelectric actuator patch whose ends are located at r_{1j} and r_{2j}. Suppose the point r_{1j} is in the element n_{1j} whose corresponding local position is r_{1j_e}. Similarly, the r_{2j} is in the element n_{2j} whose corresponding local position is r_{2j_e}.

The virtual work done by the whole structure $\delta\overline{W}_j(t)$ due to the j^{th} actuator excitation can be calculated by using (2.76), (2.96) and the Dirac delta function property (2.78) as follows:

$$\begin{aligned}
\delta\overline{W}_j(t) &= \int_0^L \frac{\partial^2 M_{prj}}{\partial r^2}\,\delta w(t,r)\,dr \\
&= \int_0^L K_j\,V_{aj}(t)\left[\frac{d\delta(r-r_{1j})}{dr} - \frac{d\delta(r-r_{2j})}{dr}\right]\delta w(t,r)\,dr \\
&= K_j\,V_{aj}(t)\left[\frac{\partial\delta w(t,r_{2j})}{\partial r} - \frac{\partial\delta w(t,r_{1j})}{\partial r}\right] \\
&= K_j\,V_{aj}(t)\left[\frac{d\bar{H}(r_{2j_e})^T}{dr_e}\,A_{n_{2j}} - \frac{d\bar{H}(r_{1j_e})^T}{dr_e}\,A_{n_{1j}}\right]\delta w(t) \\
&= \hat{F}_j(t)^T\,\delta w(t)
\end{aligned} \tag{2.97}$$

where $\hat{F}_j(t) \in \mathbf{R}^{k\times 1}$ denotes the global nodal force vector of the beam. Hence,

$$\begin{aligned}
\hat{F}_j(t) &= K_j\,V_{aj}(t)\left[A_{n_{2j}}^T\,\frac{d\bar{H}(r_{2j_e})}{dr_e} - A_{n_{1j}}^T\,\frac{d\bar{H}(r_{1j_e})}{dr_e}\right] \\
&= K_j\,V_{aj}(t)\,\Theta_j \\
&= \bar{F}_j\,V_{aj}(t)
\end{aligned} \tag{2.98}$$

where $\bar{F}_j, \Theta_j \in \mathbf{R}^{k\times 1}$.

If the contribution of all J actuators are considered, we have

$$\begin{aligned}
\hat{F}(t) &= \sum_{j=1}^{J} \bar{F}_j\,V_{aj}(t) \\
&= \bar{F}\,V_a(t)
\end{aligned} \tag{2.99}$$

where $V_a = [V_{a1}\ldots V_{aJ}]^T$ and $\bar{F} = [\bar{F}_1\ldots\bar{F}_J] \in \mathbf{R}^{k\times J}$.

2.7.2 Global equation of motion

The global equation of motion defines the equation of motion of the overall structure. Substituting the transformation (2.95) to (2.93) and (2.94) gives the contribution of the n^{th} element to the global mass matrix $\hat{M}$ and global stiffness matrix $\hat{K}$. Matrices $\hat{M}$ and $\hat{K}$ are then obtained from the contribution of each

element to the total kinetic energy and strain energy respectively:

$$\hat{M} = \sum_{n=1}^{N} A_n^T M_{e_n} A_n \tag{2.100}$$

$$\hat{K} = \sum_{n=1}^{N} A_n^T K_{e_n} A_n \tag{2.101}$$

where $\hat{M}, \hat{K} \in \mathbf{R}^{k \times k}$.

The global equation of motion of the FE beam can now be obtained as:

$$\hat{M}\ddot{w}(t) + \hat{K}w(t) = \hat{F}(t). \tag{2.102}$$

The eigenvalue problem from the above formulation is

$$\hat{K}w(t) = \lambda \hat{M}\, w(t) \tag{2.103}$$

where λ represents an eigenvalue of the system. The set of normalized eigenvectors $\Phi = [\phi_1 \;\; \phi_2 \ldots \phi_k]$ has the following orthogonality properties:

$$\Phi^T \hat{M}\, \Phi = I \tag{2.104}$$

$$\Phi^T \hat{K}\, \Phi = \Lambda \tag{2.105}$$

where I is a unit matrix and $\Lambda = \mathrm{diag}(\omega_1^2 \;\; \omega_2^2 \ldots \omega_k^2)$. Here, $\Phi \in \mathbf{R}^{k \times k}$ and $\phi_i \in \mathbf{R}^{k \times 1}$. Incorporating a new state q and using a linear transformation

$$w(t) = \Phi\, q(t) \tag{2.106}$$

the equation of motion in (2.102) can be transformed into

$$\begin{aligned} \Phi^T \hat{M}\, \Phi\, \ddot{q}(t) + \Phi^T \hat{K}\, \Phi\, q(t) &= \Phi^T \hat{F}(t) \\ \ddot{q}(t) + \Lambda\, q(t) &= \Phi^T \hat{F}(t). \end{aligned} \tag{2.107}$$

The above formulation uses the orthogonality properties of the eigenvectors Φ in (2.104) and (2.105). The equation of motion (2.107) represents the uncoupled equations of motion of the beam. Since flexible structures have relatively small damping, a proportional damping $\hat{D}$ can be conveniently included into the equation of motion where $\hat{D} = \mathrm{diag}(2\zeta_1\omega_1 \ldots 2\zeta_k\omega_k)$ and ζ_i is the damping

factor associated with mode i. Therefore, the damped equation of motion for the beam is

$$\ddot{q}(t) + \hat{D}\,\dot{q}(t) + \Lambda\, q(t) = \Phi^T\,\hat{F}(t). \tag{2.108}$$

After obtaining the equation of motion of the FE piezoelectric laminate beam, the transfer function of the system can be determined. Consider again the transverse deflection w given in (2.96). Using the linear transformation $w = \Phi\, q$ in (2.106):

$$\begin{aligned} w(t,r) &= C_w(r)\,\Phi\, q(t) \\ &= \sum_{i=1}^{k} C_w(r)\,\phi_i\, q_i(t). \end{aligned} \tag{2.109}$$

Taking the Laplace transform of the equation of motion for each mode i from (2.108) and using (2.99):

$$\begin{aligned} (s^2 + 2\zeta_i\omega_i s + \omega_i^2)\, q_i(s) &= \phi_i^T\,\hat{F}(s) \\ &= \phi_i^T\,\bar{F}\,V_a(s). \end{aligned} \tag{2.110}$$

Realizing that the Laplace transform of the deflection is

$$w(s,r) = \sum_{i=1}^{k} C_w(r)\phi_i q_i(s)$$

then the transfer function from $V_a(s)$ to $w(s,r)$ is

$$G_r(s,r) = \sum_{i=1}^{k} \frac{C_w(r)\,\phi_i\,\phi_i^T\,\bar{F}}{s^2 + 2\zeta_i\omega_i s + \omega_i^2} \tag{2.111}$$

where $\bar{F} = [K_1\Theta_1 \ldots K_J\Theta_j]$ from (2.98).

2.7.3 Piezoelectric sensors

We consider the use of piezoelectric sensors for the beam. The derivations follow from Section 2.6. Integrating the charge q_p (2.85) over the length of the sensor, the k^{th} sensor voltage is

$$V_{sk}(t) = \Omega_k \int_{r_{1k}}^{r_{2k}} \frac{\partial^2 w}{\partial r^2}\, dr \tag{2.112}$$

where Ω_k is defined in (2.88). The integral given in the above equation can be evaluated as:

$$\begin{aligned}\int_{r_{1k}}^{r_{2k}} \frac{\partial^2 w(t,r)}{\partial r^2}\, dr &= \left[\frac{\partial w(t,r)}{\partial r}\right]_{r_{1k}}^{r_{2k}} \\ &= \left[\frac{\partial w(t,r_{2k})}{\partial r} - \frac{\partial w(t,r_{1k})}{\partial r}\right] \\ &= \left[\frac{d\bar{H}(r_{2k_e})^T}{dr_e} A_{n_{2k}} - \frac{d\bar{H}(r_{1k_e})^T}{dr_e} A_{n_{1k}}\right] w(t) \\ &= \Theta_k^T\, w(t) \end{aligned} \tag{2.113}$$

where Θ_k is described in (2.98) by replacing j with k. From (2.112), the sensor output $V_s = [V_{s1} \ldots V_{sJ}]^T$ is

$$\begin{aligned} V_s(t) &= \begin{bmatrix} \Omega_1 \Theta_1^T \\ \vdots \\ \Omega_J \Theta_J^T \end{bmatrix} w(t) \\ &= \hat{\Theta}\, w(t) \end{aligned} \tag{2.114}$$

where $\hat{\Theta} \in \mathbf{R}^{J \times k}$.

Using a new state q in (2.106), the transfer function from the actuator voltage $V_a(s)$ to sensor voltage $V_s(s)$ is

$$G_{Vs}(s) = \sum_{i=1}^{k} \frac{\hat{\Theta}\phi_i \phi_i^T \bar{F}}{s^2 + 2\zeta_i\, \omega_i\, s + \omega_i^2}. \tag{2.115}$$

2.8 Summary

Modal analysis can be used to obtain exact solutions to PDE's that govern the dynamics of flexible structures. In our case, we can assume uniform structures with reasonable accuracy since the piezoelectric patches used are relatively thin with respect to dimensions of the structures. Thus, modal analysis can be used to model such systems with certain boundary conditions. In general cases of smart structures, approximate methods such as the FE method may be required. There are other more comprehensive methods for modelling piezoelectric

laminate structures, such as [BSW96, Yu96]. The modelling includes the contribution of piezoelectric patches to the properties of the structures and non-linear modelling of piezoelectric structures. Our task in this thesis is to obtain reasonable and usable models that can be used for control design. The modelling approach described in this chapter is sufficient to model piezoelectric laminate structures that are used in our experiments.

The spatial information conveyed in the systems can be used to design controllers that minimize structural vibration in a spatially-averaged sense. The issue will be discussed later in this thesis.

Chapter 3

Spatial norms

This thesis deals with analysis and control of spatially distributed systems. Standard performance measures such as $\mathcal{H}_2$ and $\mathcal{H}_\infty$ norms can be used for this purpose. However, we intend to use performance measures that conveniently incorporate the spatial information of the systems, i.e. spatial norms. The concept of spatial norms is proposed in [MPP99, MF98] and will be used throughout this thesis for model correction, optimal placement and control design of smart structures. Hence, it is necessary to discuss some important concepts of spatial norms in this chapter, concentrating on spatially distributed LTI systems.

3.1 Spatial $\mathcal{H}_2$ norm

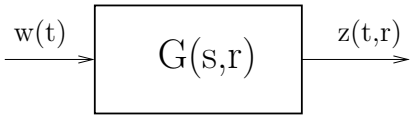

Figure 3.1: A spatially distributed system

Consider a system G in Figure 3.1 that maps an input signal $w \in \mathbf{R}^m$ to an output signal $z \in \mathbf{R}^\ell \times \mathcal{R}$. The outputs are spatially distributed over a set $\mathcal{R}$.

The following definitions are proposed in [MPP99, MF98]:

Definition 3.1 Spatial $\mathcal{H}_2$ norm of a signal: *the spatial $\mathcal{H}_2$ norm of a signal $z \in \mathbf{R}^\ell \times \mathcal{R}$ is defined as:*

$$\ll z \gg_2^2 = \int_0^\infty \int_{\mathcal{R}} z(t,r)^T z(t,r) dr dt \tag{3.1}$$

The spatial $\mathcal{H}_2$ norm of z can be regarded as the energy of the spatially distributed signal z. In flexible structures, the signal can be represented as the deflection/deformation at every point along the structure.

Definition 3.2 Spatial $\mathcal{H}_2$ norm of a system: *The spatial $\mathcal{H}_2$ norm of a stable system $G(s,r)$ with $r \in \mathcal{R}$ is defined as:*

$$\ll G(s,r) \gg_2^2 = \frac{1}{2\pi} \int_{-\infty}^{\infty} \int_{\mathcal{R}} tr\{G(j\omega,r)^* G(j\omega,r)\} dr d\omega \tag{3.2}$$

The spatial $\mathcal{H}_2$ norm of the system takes into account the spatial information embedded in the system. We will use this concept to develop spatial controllers for minimizing structural vibration in Chapters 6 and 7.

An alternative way to calculate the spatial $\mathcal{H}_2$ norm of a system is by finding an equivalent finite-dimensional system. The $\mathcal{H}_2$ norm of the finite-dimensional system will be similar to the spatial $\mathcal{H}_2$ norm of the original system. Therefore, we only need to find the $\mathcal{H}_2$ norm of the equivalent system using a standard computation technique [ZDG96].

To be clearer, we consider a state-space form of a spatially distributed model G:

$$\begin{aligned} \dot{x}(t) &= Ax(t) + Bu(t) \\ y(t,r) &= C(r)x(t). \end{aligned} \tag{3.3}$$

The spatial $\mathcal{H}_2$ norm of a system of the form (3.3) can be shown to be equivalent to the $\mathcal{H}_2$ norm of a finite-dimensional system via the following theorem [MF98]:

Theorem 3.1 *Consider a stable system with a transfer function matrix $G(s,r)$ that can be described in state-space form by (3.3). Then*

$$\ll G(s,r) \gg_2 = \|\tilde{G}(s)\|_2$$

where $\tilde{G}(s)$ is a finite-dimensional system defined by

$$\tilde{G}(s) = \Gamma(sI - A)^{-1}B$$

and

$$\Gamma^T\Gamma = \int_{\mathcal{R}} C(r)^T C(r)dr. \tag{3.4}$$

When we deal with models that arise from modal analysis, the computation of the spatial $\mathcal{H}_2$ norm of such systems can be simplified due to the orthogonality property of the associated eigenfunctions. Consider a typical modal analysis model:

$$G(s,r) = \sum_{i=1}^{\infty} \frac{\phi_i(r)P_i}{s^2 + 2\zeta_i\omega_i s + \omega_i^2} \tag{3.5}$$

where $r \in \mathcal{R}$ and $P_i \in \mathbf{R}^{1\times n}$ for systems with n inputs.

The orthogonality condition of the eigenfunctions for structures with uniform properties can be expressed as:

$$\int_{\mathcal{R}} \phi_i(r)\phi_j(r)dr = \delta_{ij}. \tag{3.6}$$

The following theorem will be useful in computing the spatial $\mathcal{H}_2$ norm of such a system [MF98]:

Theorem 3.2 *Consider the system $G(s,r)$ in (3.5) and suppose that the eigenfunctions satisfy the orthogonality condition in (3.6), then*

$$\ll G(s,r) \gg_2^2 = \sum_{i=1}^{\infty} \|\tilde{G}_i(s)\|_2^2 \tag{3.7}$$

where

$$\tilde{G}_i(s) = \frac{P_i}{s^2 + 2\zeta_i\omega_i s + \omega_i^2}. \tag{3.8}$$

This theorem proves that the spatial $\mathcal{H}_2$ norm of a spatially distributed system of the form (3.5) with the orthogonality condition (3.6) is equivalent to the $\mathcal{H}_2$ norm of another system.

We consider that the system in (3.5) is truncated to include only the first N modes so that the truncated model is G_N. Based on Theorem 3.2, the approximate spatial $\mathcal{H}_2$ norm of the system can also be calculated as:

$$\ll G_N(s,r) \gg_2^2 = \sum_{i=1}^{N} \|\tilde{G}_i(s)\|_2^2.$$

For general cases of systems that do not satisfy (3.6), the spatial $\mathcal{H}_2$ norm of the system can be evaluated numerically, such as by using the state-space method in Theorem 3.1.

In more general cases, it may be beneficial to include a spatial weighting function to emphasize certain spatial regions within the set $\mathcal{R}$. For example, we may want to emphasize controlling vibration over a specific region of a structure. Hence, by placing a suitable spatial weighting function, a certain region can be emphasized. Definitions 3.1 and 3.2 can be extended to allow such spatial weightings [MF98] as follows:

Definition 3.3 Weighted spatial $\mathcal{H}_2$ norm of a signal: *Consider a signal $z(t,r) \in \mathbf{R}^\ell \times \mathcal{R}$. Then, the weighted spatial $\mathcal{H}_2$ norm of z is defined as:*

$$\ll z \gg_{2,Q}^2 = \int_0^\infty \int_{\mathcal{R}} z(t,r)^T Q(r) z(t,r) dr dt \tag{3.9}$$

where $Q(r) \geq 0$.

Definition 3.4 Weighted spatial $\mathcal{H}_2$ norm of a system: *Consider a stable system $G(s,r)$ with $r \in \mathcal{R}$. The weighted spatial $\mathcal{H}_2$ norm of this system is defined as:*

$$\ll G(s,r) \gg_{2,Q}^2 = \frac{1}{2\pi} \int_{-\infty}^{\infty} \int_{\mathcal{R}} tr\{G(j\omega,r)^* Q(r) G(j\omega,r)\} dr d\omega \tag{3.10}$$

where $Q(r) \geq 0$.

Suppose $Q(r)$ is chosen to be a Dirac delta function $Q(r) = \delta(r - r_1)$ with $r_1 \in \mathcal{R}$. Then (3.10) becomes

$$\ll G(s,r) \gg_{2,\delta}^2 = \frac{1}{2\pi} \int_{-\infty}^{\infty} \mathrm{tr}\{G(j\omega, r_1)^* G(j\omega, r_1)\} d\omega.$$

The above norm is simply the $\mathcal{H}_2$ norm of the system G at $r = r_1$. Theorem 3.2 cannot be used to compute the weighted spatial $\mathcal{H}_2$ norm of a system because the orthogonality condition in (3.6) is not applicable, unless $Q(r)$ is a constant. Alternatively, the weighted spatial $\mathcal{H}_2$ norm of a system can be computed via state-space form as in Theorem 3.1. In this case, Γ is computed via

$$\Gamma^T \Gamma = \int_{\mathcal{R}} C(r)^T \, Q(r) \, C(r) dr. \tag{3.11}$$

3.2 Spatial $\mathcal{H}_\infty$ norm

An alternative performance measure that is commonly used in control theory is the $\mathcal{H}_\infty$ norm. The concept of $\mathcal{H}_\infty$ norm has a significant role in robust control theory. Since this norm satisfies the multiplicative property of a norm, it can be conveniently used to incorporate model uncertainties [SP96]. We now consider the extension of this $\mathcal{H}_\infty$ norm for spatially distributed systems. This section will discuss the concept of spatial $\mathcal{H}_\infty$ norm for spatially distributed LTI systems, proposed in [MPP99]. Later, in Chapter 8, we will use this concept to design spatial $\mathcal{H}_\infty$ controllers for smart structures.

Definition 3.5 Spatial induced norm of a system: *Consider a stable system $G(s,r)$. Let $\mathcal{G}$ be the linear operator which maps the inputs of $G(s,r)$ to its outputs. The spatial induced norm of $\mathcal{G}$ is*

$$\ll \mathcal{G} \gg^2 = \sup_{0 \neq w \in \mathcal{L}_{2[0,\infty]}} \frac{\ll z \gg_2^2}{\|w\|_2^2}. \tag{3.12}$$

Definition 3.6 Spatial $\mathcal{H}_\infty$ norm of a system: *The spatial $\mathcal{H}_\infty$ norm of a stable system $G(s,r)$ is*

$$\ll G \gg_\infty^2 = \sup_{\omega \in \mathbf{R}} \lambda_{\max} \left(\int_{\mathcal{R}} G(j\omega, r)^* G(j\omega, r) dr \right) \tag{3.13}$$

where $\lambda_{max}(F)$ is the largest eigenvalue of the matrix F.

The next theorem shows that the spatial $\mathcal{H}_\infty$ norm of $G(s,r)$ is equivalent to the spatial induced norm of $\mathcal{G}$ [MPP99].

Theorem 3.3 *Suppose a stable system has a transfer function matrix $G(s,r)$ and let $\mathcal{G}$ denotes the linear map it induces from the $\mathcal{L}_2$ spaces of its inputs to its infinite-dimensional outputs. Its induced operator norm $\ll \mathcal{G} \gg$ satisfies*

$$\ll \mathcal{G} \gg = \ll G \gg_\infty .$$

Similar to the case of weighted spatial $\mathcal{H}_2$ norm, a spatial weighting function can be included in the calculation of the spatial $\mathcal{H}_\infty$ norm of the system. The definitions are as follows:

Definition 3.7 Weighted spatial induced norm of a system: *Let $\mathcal{G}$ be the linear operator which maps the inputs of $G(s,r)$ to its outputs. The weighted spatial induced norm of $\mathcal{G}$ is*

$$\ll \mathcal{G} \gg_Q^2 = \sup_{0 \neq w \in \mathcal{L}_{2[0,\infty]}} \frac{\ll z \gg_{2,Q}^2}{\|w\|_2^2}. \tag{3.14}$$

Definition 3.8 Weighted spatial $\mathcal{H}_\infty$ norm of a system: *Consider a stable system $G(s,r)$ with $r \in \mathcal{R}$. The weighted spatial $\mathcal{H}_\infty$ norm of this system is*

$$\ll G \gg_{\infty,Q}^2 = \sup_{\omega \in \mathbf{R}} \lambda_{\max} \left(\int_{\mathcal{R}} G(j\omega, r)^* Q(r) G(j\omega, r) dr \right). \tag{3.15}$$

It is straightforward to show that Theorem 3.3 holds for weighted spatial norms. That is

$$\ll \mathcal{G} \gg_Q = \ll G \gg_{\infty,Q} .$$

Hence, the spatial $\mathcal{H}_2$ and $\mathcal{H}_\infty$ norms take into account the spatial information of the spatially distributed systems such as flexible structures. We can use these spatial norms as performance measures in model correction, optimal placement and control design of smart structures.

Chapter 4

Model correction

In modal analysis, smart structure models can be represented by an infinite number of modes. In control design, we are usually interested in controlling vibration for a particular bandwidth. Low frequency modes tend to contribute more significantly to structural vibration than high frequency modes. However, it is known that high frequency (out-of-bandwidth) modes also contribute to the dynamics at low frequencies (in-bandwidth). Thus, a sufficient number of out-of-bandwidth modes may need to be included to obtain a reasonably accurate in-bandwidth model [Hug87].

The inclusion of out-of-bandwidth modes in the model may yield a system with a relatively higher order. Many modern control design methods produce a controller with similar order to that of the plant. This may yield a controller with an excessive order that may not be practical to be implemented to real systems. We can reduce the order of the controller but the order reduction must be done with care since the reduced-order controller may adversely affect the closed-loop performance and stability. Thus, it can be convenient to reduce the order of the model first so as to include only necessary modes within the control bandwidth.

There are several approaches that can be used for model reduction. We can use direct truncation, assuming the collective impact of out-of-bandwidth modes on the in-bandwidth dynamics is minor. However, the removal of the

out-of-bandwidth modes may perturb the in-bandwidth zeros [Cla97, Moh00a, Moh00b, MH00]. Furthermore, the gain at zero-frequency (DC gain) is also perturbed. The truncation error can be significant, especially for cases where actuators and sensors are collocated.

One particular approach to compensate for the truncation error is to add a correction term into the truncated model. The mode acceleration approach in the aeroelasticity literature adds a feedthrough term to compensate for the DC contents of out-of-bandwidth modes [BA75]. The approach has been recently revisited in [Cla97, Moh00a, Moh00b, MH00]. However, this approach only reduces the DC error to zero. The error at higher frequencies, within the bandwidth of interest, could still be large. It is also not clear how the multivariable systems should be dealt with.

The extension of the mode acceleration approach is discussed in [Moh00b, Moh00a]. An optimal feedthrough term is determined by minimizing the weighted $\mathcal{H}_2$ norm of the truncation error. The existence of an analytical solution for the optimal feedthrough term for multivariable pointwise models allows the solution to be used directly. For spatial models, the approach is proposed in [Moh00a] by finding a feedthrough term that minimizes the weighted spatial $\mathcal{H}_2$ norm of the truncation error. In [Moh00b, Moh00a], however, it is assumed that there is no damping in the system. This may be sufficient if the damping is relatively small, but the solution may not be close to optimality if the damping is considerable.

In this chapter, we will briefly mention previous approaches in [Moh00b, Moh00a, MH00] for obtaining the optimal feedthrough terms for systems that assume no damping. Later, we will extend the approach for systems that include damping via convex optimization and analytical optimization.

4.1 Model correction without damping effect

We discuss the determination of optimal feedthrough terms for pointwise and spatial models. The main assumption here is that there is no damping in the

system. This may be an acceptable assumption since many resonant systems have relatively small damping. For example, flexible structures have typical damping ratios ranging in the order of 0.01 or 0.001. We consider the model correction for pointwise and spatial models of resonant systems based on the approaches in [Moh00b, Moh00a].

Consider a typical MIMO model of a resonant system that is obtained from modal analysis:

$$G(s) = \sum_{i=1}^{\infty} \frac{P_i}{s^2 + \omega_i^2} \tag{4.1}$$

where $P_i \in \mathbf{R}^{m \times n}$. Hence, G maps the input $u \in \mathbf{R}^n$ to the output $y \in \mathbf{R}^m$. This model represents the pointwise model of the system that relates n input signals to m output signals.

The obvious way to reduce the order of the model is by direct truncation. Suppose only N lowest frequency modes inside the bandwidth of interest (i.e. in-bandwidth modes) are included in the model, then

$$G_N(s) = \sum_{i=1}^{N} \frac{P_i}{s^2 + \omega_i^2}. \tag{4.2}$$

Higher frequency modes (out-of-bandwidth modes) are ignored assuming that their effects on the in-bandwidth dynamics are minor. However, this direct truncation perturbs the zero locations and the DC content of the truncated model, especially when the system has a collocated nature [Cla97, Moh00a, Moh00b, MH00]. From (4.1), it can be observed that the DC contribution of each mode is P_i/ω_i^2. Thus, the removal of high frequency modes leads to error in DC content of the truncated model. It is obvious that the error will be more significant if the system is collocated. For instance, a SISO (Single-Input, Single-Output) collocated system contains P_i/ω_i^2 terms with similar signs. Hence, the error in DC content will be accumulated from each mode. The truncation error may affect the robustness of the closed-loop system when a feedback controller is designed. The approach that is proposed in [Moh00b] is to find an analytical solution for an optimal feedthrough term to compensate for the truncation error via $\mathcal{H}_2$ norm approach. The results will be presented here.

4.1.1 $\mathcal{H}_2$ norm approach

Consider the pointwise system whose truncated model is given in (4.2). The approach is based on finding a suitable feedthrough term, which is a constant matrix $K \in \mathbf{R}^{m\times n}$, to compensate for the truncation error resulting from the removal of modes $N+1$ to ∞. The corrected model $\hat{G}$ then can be written as:

$$\hat{G}(s) \;=\; G_N(s) + K. \tag{4.3}$$

The matrix K is determined by finding K that minimizes the weighted error between the full-order model and the corrected model. The cost function is defined as:

$$J \;=\; \|W(s)(G(s) - \hat{G}(s))\|_2^2 \tag{4.4}$$

with W a diagonal matrix whose diagonal elements are ideal low-pass filters:

$$W = \mathrm{diag}(w \;\; w \ldots w) \tag{4.5}$$

and

$$w(j\omega) \;=\; \begin{cases} 1 & -\omega_c \le \omega \le \omega_c \\ 0 & \text{otherwise} \end{cases} \tag{4.6}$$

in which $\omega_c \in (\omega_N, \omega_{N+1})$ is the cut-off frequency of each filter.

The optimum value K_{opt} can be shown to be [Moh00b]:

$$K_{opt} \;=\; \frac{1}{2\omega_c} \sum_{i=N+1}^{\infty} \frac{1}{\omega_i} \ln\left(\frac{\omega_i + \omega_c}{\omega_i - \omega_c}\right) P_i. \tag{4.7}$$

The solution gives the analytical solution for the optimal feedthrough term for pointwise models.

4.1.2 Spatial $\mathcal{H}_2$ norm approach

Now, we consider finding optimal feedthrough terms for spatial models. The approach for compensating the truncated model of such systems will be useful when we deal with the spatial control of smart structures in the next few chapters. We will mention the approach proposed in [Moh00a].

The spatial model of a resonant system can be represented by

$$G_r(s,r) \;=\; \sum_{i=1}^{\infty} \frac{\phi_i(r)P_i}{s^2+\omega_i^2} \tag{4.8}$$

where $P_i \in \mathbf{R}^{1\times n}$ and the transfer function G_r maps the input $u \in \mathbf{R}^n$ to the output $y \in \mathbf{R}\times\mathcal{R}$, where $r \in \mathcal{R}$. For instance, $\mathcal{R}=[0,L]$ for a beam with length L, and $\mathcal{R}=[0,a]\times[0,b]$ for a plate with size $a\times b$. For a beam under flexural vibration, the spatial output y is the transverse displacement at point r along the beam. Also, ϕ_i is the eigenfunction associated with mode i which is assumed to satisfy the orthogonality property in (3.6).

By direct truncation, the truncated spatial model is

$$G_{rN}(s,r) \;=\; \sum_{i=1}^{N} \frac{\phi_i(r)P_i}{s^2+\omega_i^2}. \tag{4.9}$$

A feedthrough term K_r is added to the truncated model G_{rN} to compensate for the truncation error. The corrected model is

$$\hat{G}_r(s,r) \;=\; G_{rN}(s,r)+K_r(r) \tag{4.10}$$

and K_r is chosen in the following form:

$$K_r(r) \;=\; \sum_{i=N+1}^{\infty} \phi_i(r)K_{ri} \tag{4.11}$$

where $K_{ri} \in \mathbf{R}^{1\times n}$.

Next, K_{ri} is determined such that the spatial $\mathcal{H}_2$ norm of the weighted error between the full-order model (4.8) and the corrected model (4.10) is minimized. The cost function is defined as:

$$\begin{aligned} J_r \;&=\; \ll W_r(s,r)(G_r(s,r)-\hat{G}_r(s,r)) \gg_2^2 \\ &=\; \ll W_r(s,r)(\tilde{G}_r(s,r)-K_r(r)) \gg_2^2 \end{aligned} \tag{4.12}$$

where

$$\tilde{G}_r(s,r) \;=\; \sum_{i=N+1}^{\infty} \frac{\phi_i(r)P_i}{s^2+\omega_i^2}. \tag{4.13}$$

Here, W_r is a diagonal matrix whose elements are ideal low-pass filters distributed spatially over $\mathcal{R}$ [Moh00a]:

$$W_r = \text{diag}(w_r \quad w_r \ldots w_r) \tag{4.14}$$

where

$$w_r(j\omega, r) \quad = \quad \begin{cases} 1 & -\omega_c \leq \omega \leq \omega_c, r \in \mathcal{R} \\ 0 & \text{otherwise} \end{cases} \tag{4.15}$$

and $\omega_c \in (\omega_N, \omega_{N+1})$ is the cut-off frequency of each low-pass filter.

It is shown in [Moh00a], that the cost function in (4.12) can be minimized by using the orthogonality property of the eigenfunctions (3.6). The optimal K_{ri} is

$$K_{ri}^{opt} \quad = \quad \frac{1}{2\omega_c\omega_i} \ln\left(\frac{\omega_i + \omega_c}{\omega_i - \omega_c}\right) P_i. \tag{4.16}$$

4.1.3 Spatial $\mathcal{H}_\infty$ approach

Another way to obtain the feedthrough term is to find the optimal feedthrough term using spatial $\mathcal{H}_\infty$ norm as a performance measure. The approach is proposed in [MH00] and only the results will be presented here.

The optimal feedthrough term is calculated such that the following cost function is minimized:

$$\begin{aligned} J_r \quad &= \quad \ll W_r(s,r)(G_r(s,r) - \hat{G}_r(s,r)) \gg_\infty^2 \\ &= \quad \ll W_r(s,r)(\tilde{G}_r(s,r) - K_r(r)) \gg_\infty^2 \end{aligned} \tag{4.17}$$

where all parameters have been mentioned previously in Section 4.1.2.

It can be shown that the optimal feedthrough term has the form of [MH00]

$$K_r^{opt}(r) = \sum_{i=N+1}^{\infty} \phi_i(r) K_{ri}^{opt} \tag{4.18}$$

with

$$K_{ri}^{opt} = \frac{1}{2}\left(\frac{1}{\omega_i^2} + \frac{1}{\omega_i^2 - \omega_c^2}\right) P_i. \tag{4.19}$$

4.2 Model correction with damping effect via convex optimization

In this section, we will develop a procedure for minimizing the truncation error when the systems have considerable damping associated with each mode. The approach is to set up a convex optimization problem and solve it using the convex optimization techniques [BEGFB94].

Consider a general multivariable pointwise model of the following form:

$$G_M(s) = \sum_{i=1}^{M} \frac{\Xi_i}{s^2 + 2\zeta_i\omega_i s + \omega_i^2} \tag{4.20}$$

where $\Xi_i \in \mathbf{R}^{m\times n}$. The model can be obtained from modal analysis or other methods.

This model is truncated by keeping the first $N < M$ modes:

$$G_N(s) = \sum_{i=1}^{N} \frac{\Xi_i}{s^2 + 2\zeta_i\omega_i s + \omega_i^2}. \tag{4.21}$$

A feedthrough term is added to (4.21) to correct the truncated model. The corrected model is

$$\hat{G}_N(s) = \sum_{i=1}^{N} \frac{\Xi_i}{s^2 + 2\zeta_i\omega_i s + \omega_i^2} + K \tag{4.22}$$

where $K \in \mathbf{R}^{m\times n}$.

The optimal K, i.e. K^{opt}, is determined from the following minimization:

$$\begin{aligned} J_2 &= \min_{K\in\mathbf{R}^{m\times n}} \|W(s)(G_M(s) - \hat{G}_N(s))\|_2^2 \\ &= \min_{K\in\mathbf{R}^{m\times n}} \|E(s)\|_2^2 \end{aligned} \tag{4.23}$$

where E is the error system and W is a low-pass weighting function whose purpose is to emphasize the in-bandwidth error. The cut-off frequency of this filter is typically chosen to lie within the range $\omega_N \le \omega \le \omega_{N+1}$.

The above transfer functions can be written in state-space form:

$$G_N(s) = \left[\begin{array}{c|c} A & B \\ \hline C & 0 \end{array}\right]$$

$$
\begin{aligned}
G_M(s) &= \left[\begin{array}{cc|c} A & 0 & B \\ 0 & A_2 & B_2 \\ \hline C & C_2 & 0 \end{array}\right] \\
W(s) &= \left[\begin{array}{c|c} A_w & B_w \\ \hline C_w & 0 \end{array}\right]
\end{aligned} \tag{4.24}
$$

with appropriate values for A, B, C, A_2, B_2, C_2 ,A_w, B_w and C_w.

Using the above notation, an expression for the error system is

$$
\begin{aligned}
E(s) &= W(s)\left(G_M(s) - \hat{G}_N(s)\right) \\
&= \left[\begin{array}{c|c} A_w & B_w \\ \hline C_w & 0 \end{array}\right] \times \left(\left[\begin{array}{cc|c} A & 0 & B \\ 0 & A_2 & B_2 \\ \hline C & C_2 & 0 \end{array}\right] - \left[\begin{array}{c|c} A & B \\ \hline C & K \end{array}\right] \right) \\
&= \left[\begin{array}{c|c} A_w & B_w \\ \hline C_w & 0 \end{array}\right] \times \left[\begin{array}{c|c} A_2 & B_2 \\ \hline C_2 & -K \end{array}\right] \\
&= \left[\begin{array}{cc|c} A_w & B_w C_2 & -B_w K \\ 0 & A_2 & B_2 \\ \hline C_w & 0 & 0 \end{array}\right] \\
&= \left[\begin{array}{c|c} \bar{A} & \bar{B}_1 K + \bar{B}_2 \\ \hline \bar{C} & 0 \end{array}\right]
\end{aligned} \tag{4.25}
$$

where

$$
\begin{aligned}
\bar{A} &= \left[\begin{array}{cc} A_w & B_w C_2 \\ 0 & A_2 \end{array}\right] \\
\bar{B}_1 &= \left[\begin{array}{c} -B_w \\ 0 \end{array}\right] \\
\bar{B}_2 &= \left[\begin{array}{c} 0 \\ B_2 \end{array}\right] \\
\bar{C} &= \left[\begin{array}{cc} C_w & 0 \end{array}\right].
\end{aligned} \tag{4.26}
$$

The $\mathcal{H}_2$ norm of the error system E can be expressed as [BEGFB94]:

$$\|E(s)\|_2^2 = \mathrm{tr}\left\{\bar{C}P\bar{C}^T\right\} \tag{4.27}$$

where $P = P^T > 0$ is the solution to the following Lyapunov inequality :

$$\bar{A}P + P\bar{A}^T + (\bar{B}_1K + \bar{B}_2)(\bar{B}_1K + \bar{B}_2)^T < 0. \tag{4.28}$$

Hence, the above problem can be formulated as a convex optimization problem to determine K^{opt}:

$$\begin{aligned} &\text{minimize} \quad \mathrm{tr}\left\{\bar{C}P\bar{C}^T\right\} \\ &\text{subject to} \quad \begin{bmatrix} \bar{A}P + P\bar{A}^T & \bar{B}_1K + \bar{B}_2 \\ (\bar{B}_1K + \bar{B}_2)^T & -I \end{bmatrix} < 0, \ P > 0. \end{aligned}$$

Another alternative to finding the feedthrough term is by using $\mathcal{H}_\infty$ norm of the error system as the cost function:

$$J_\infty = \min_{K \in \mathbf{R}^{m \times n}} \|W(s)(G_M(s) - \hat{G}_N(s))\|_\infty. \tag{4.29}$$

The strict bounded real lemma [PAJ91] is used to solve for the above problem.

Lemma 4.1 *[PAJ91] The following two conditions are equivalent:*

1. *A is stable and $\|C(sI - A)^{-1}B\|_\infty < \gamma$.*

2. *There exists a matrix $P > 0$ such that*

$$A^TP + PA + \frac{1}{\gamma^2}PBB^TP + C^TC < 0. \tag{4.30}$$

Lemma 4.1 implies that the inequality

$$\|\bar{C}(sI - \bar{A})^{-1}(\bar{B}_1K + \bar{B}_2)\|_\infty < \gamma$$

holds if and only if there exists a matrix $P > 0$ such that

$$\bar{A}^TP + P\bar{A} + \frac{1}{\gamma^2}P(\bar{B}_1K + \bar{B}_2)(\bar{B}_1K + \bar{B}_2)^TP + \bar{C}^T\bar{C} < 0. \tag{4.31}$$

Then (4.31) holds if and only if there exists a matrix $Q > 0$ such that

$$Q\bar{A}^T + \bar{A}Q + \frac{1}{\gamma^2}(\bar{B}_1K + \bar{B}_2)(\bar{B}_1K + \bar{B}_2)^T + Q\bar{C}^T\bar{C}Q < 0. \tag{4.32}$$

Using Schur complement [BEGFB94], (4.32) can be written as a linear matrix inequality:

$$\begin{bmatrix} Q\bar{A}^T + \bar{A}Q & Q\bar{C}^T & \bar{B}_1K + \bar{B}_2 \\ \bar{C}Q & -I & 0 \\ (\bar{B}_1K + \bar{B}_2)^T & 0 & -\gamma^2 I \end{bmatrix} < 0. \tag{4.33}$$

A convex optimization problem can then be formulated to solve the required optimization problem as follows:

$$\begin{aligned} &\text{minimize} \quad \beta \\ &\text{subject to} \quad \begin{bmatrix} Q\bar{A}^T + \bar{A}Q & Q\bar{C}^T & \bar{B}_1K + \bar{B}_2 \\ \bar{C}Q & -I & 0 \\ (\bar{B}_1K + \bar{B}_2)^T & 0 & -\beta I \end{bmatrix} < 0, \qquad Q > 0. \end{aligned}$$

4.2.1 Illustrative example

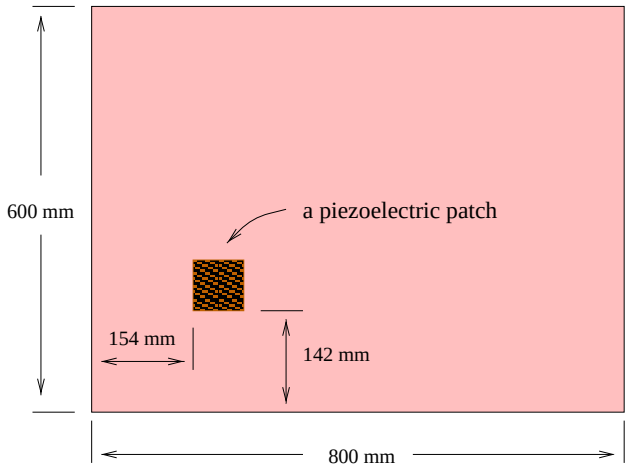

Figure 4.1: The plate model for model correction

We illustrate the use of the developed model correction procedure via a plate model. A plate model with simply-supported boundary conditions is used as the

Plate Young's modulus, E	7.0×10^{10} N/m^2
Plate Poisson's ratio, ν	0.30
Plate density, ρh	11.0 kg/m^2
Piezoceramic Young's modulus, E_p	6.20×10^{10} N/m^2
Piezoceramic Poisson's ratio, ν_p	0.30
Charge constant, d_{31}	-3.20×10^{-10} m/V
Voltage constant, g_{31}	-9.50×10^{-3} Vm/N
Capacitance, C	4.50×10^{-7} F
Electromechanical coupling factor, k_{31}	0.44

Table 4.1: Properties of the piezoelectric laminate plate

system. The structure consists of an aluminium plate of 800 mm × 600 mm × 4 mm. Two identical piezoelectric patches (72.4 mm × 72.4 mm × 0.191 mm) are used as an actuator and a sensor respectively. The patches are attached symmetrically to either side of the plate, thus collocating the actuator and sensor. The plate model is shown in Figure 4.1 and other properties are shown in Table 4.1.

A model of the structure is obtained via modal analysis technique. Only the first six modes are included in the truncated plate model G_N with $N = 6$. The feedthrough term calculation is based on the higher-order model of 25 modes G_M with $M = 25$. A low-pass filter of 4^{th} order, with the cut-off frequency of 249.7 Hz, is used in this example. The cut-off frequency is chosen to be between modes 6 and 7.

Figure 4.2 compares the frequency response (magnitude) of those two models up to the cut-off frequency. The zeros for this collocated system are shown as anti-resonances. It can be observed that the zeros of the truncated model G_N

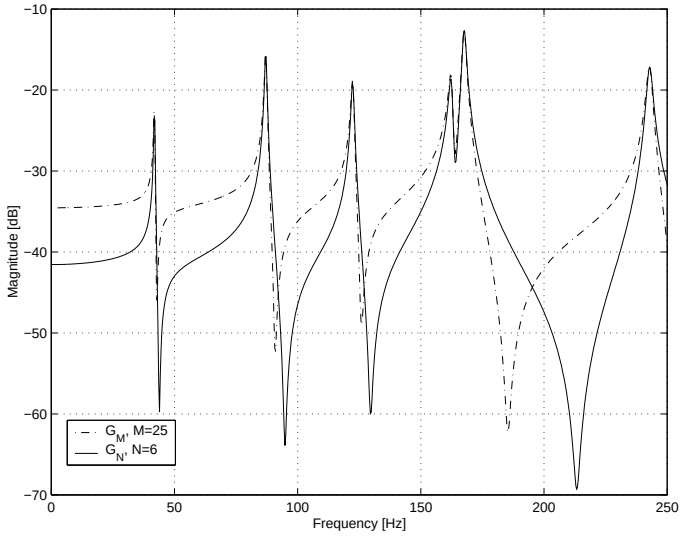

Figure 4.2: Frequency responses (magnitude) of $G_N(s)$ and $G_M(s)$

are significantly different from G_M since the effects of out-of-bandwidth modes are ignored. The zeros of G_N occur at frequencies higher than those of G_M. It is obvious that there is an error in the DC content of the truncated model since the DC contributions of out-of-bandwidth modes are removed. This truncation error can be detrimental to the closed-loop stability and performance when a feedback control is designed and implemented.

Next, we use the model correction methodology via the $\mathcal{H}_2$ norm approach. Figure 4.3 shows the corrected model $\hat{G}_N$ in comparison with the higher-order model G_M. The zeros of the corrected model now occur at frequencies closer to those of G_M. The feedthrough term also compensates for the DC error in the truncated model due to removal of out-of-bandwidth modes. The improvement of $\hat{G}_N$ compared to G_N is obvious.

We now consider compensating the truncated error via the $\mathcal{H}_\infty$ norm approach. Figure 4.4 compares the corrected model $\hat{G}_N$ and the higher-order model G_M. The feedthrough term has compensated for some truncation error due to removal of high frequency modes. However, the result for the $\mathcal{H}_\infty$ norm

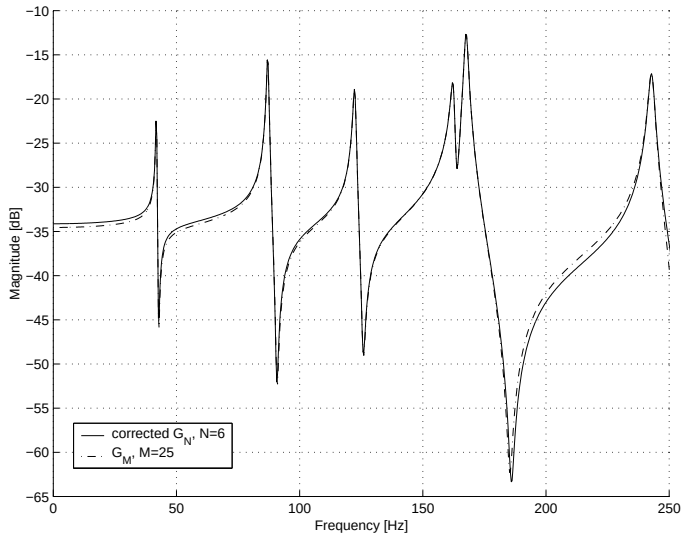

Figure 4.3: Frequency responses (magnitude) of $\hat{G}_N(s)$ and $G_M(s)$: $\mathcal{H}_2$ norm approach

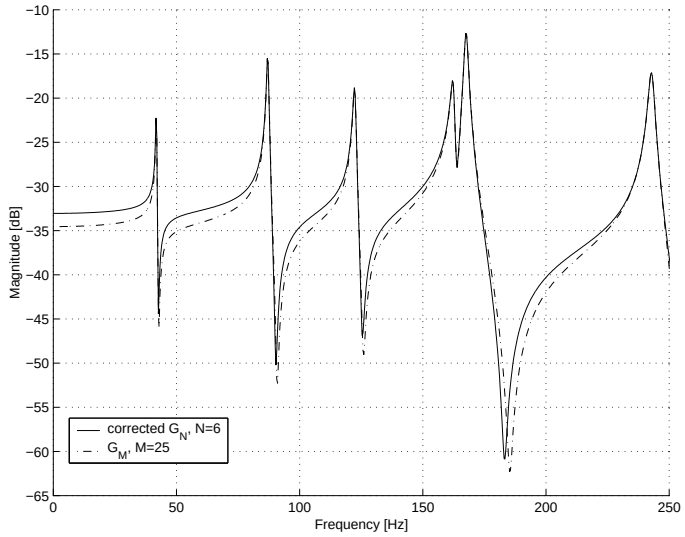

Figure 4.4: Frequency responses (magnitude) of $\hat{G}_N(s)$ and $G_M(s)$: $\mathcal{H}_\infty$ norm approach

approach, at frequencies lower than 215 Hz, is worse than that for the $\mathcal{H}_2$ norm approach (compare with Figure 4.3). To analyze the performances of both approaches, the frequency responses of the error system are plotted in Figure 4.5.

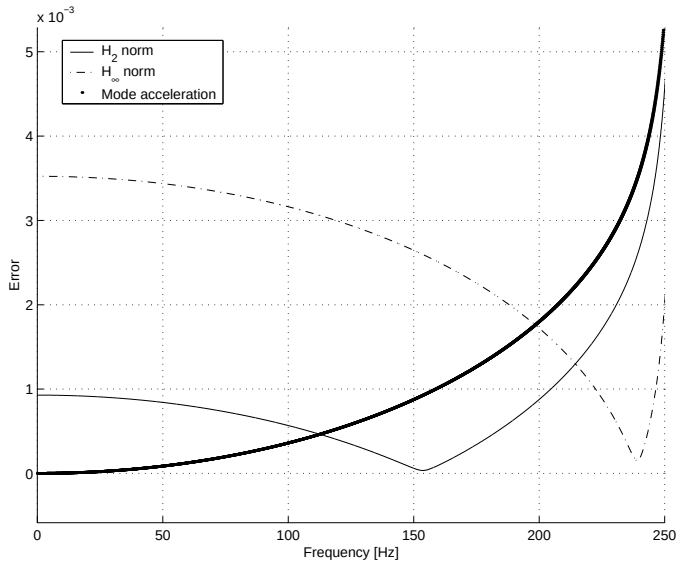

Figure 4.5: Frequency responses (magnitude) of the error system

Figure 4.5 compares the error frequency responses (magnitude) of $\mathcal{H}_2$ norm and $\mathcal{H}_\infty$ norm approaches. Up to frequency of 214.4 Hz, the error of the $\mathcal{H}_2$ norm approach is less than that of the $\mathcal{H}_\infty$ norm approach. The result is as expected since the $\mathcal{H}_2$ norm approach minimizes the error system across the frequency bandwidth. In contrast, the $\mathcal{H}_\infty$ norm approach only minimizes the $\mathcal{H}_\infty$ norm of the error system. Because a large degree of error is expected at higher frequency due to truncation of out-of-bandwidth modes, the maximum error tends to occur at a relatively high frequency. This explains the tendency of the $\mathcal{H}_\infty$ norm approach to have lower error at higher frequencies.

This implies that for improving the performance of the $\mathcal{H}_\infty$ norm approach at low frequencies, a higher order low-pass filter is desirable in order to reduce the magnitude of error at out-of-bandwidth frequencies. However, this will increase the size of the system, which will increase the computational time.

Next, we compare the performances of both approaches with the mode acceleration approach as shown in Figure 4.5. The mode acceleration approach reduces the DC error to zero as expected. However, the error increases with frequency. The error of the mode acceleration approach exceeds that of our approaches at frequencies higher than 198.4 Hz. In this case, it is reasonable to say that the performance of the $\mathcal{H}_2$ norm approach is better than those of the other two approaches at most in-bandwidth frequencies.

4.3 Model correction with damping effect via analytical approach

The previous model correction approach is based on numerical approach via convex optimization. Hence, there is a limit on the number of out-of-bandwidth modes that can be included in the optimization. The more out-of-bandwidth modes we consider, the more demanding the numerical computation will be. Moreover, the approach only deals with model correction for pointwise systems. In this section, we intend to find analytical solutions for optimal feedthrough terms for both pointwise and spatial models of resonant systems. Hence, the model correction can be done in a straightforward manner since there is no limitation on how many out-of-bandwidth modes can be included. Here, we extend the approaches proposed in [Moh00a, Moh00b] to include the effect of damping in the systems.

4.3.1 Problem statement for pointwise models

Consider a typical pointwise system with damping:

$$G(s) \;=\; \sum_{i=1}^{\infty} \frac{P_i}{s^2 + 2\zeta_i\omega_i s + \omega_i^2} \tag{4.34}$$

where $P_i \in \mathbf{R}^{m\times n}$ for a system with n inputs and m outputs. The truncated model is

$$G_N(s) \;=\; \sum_{i=1}^{N} \frac{P_i}{s^2 + 2\zeta_i\omega_i s + \omega_i^2}. \tag{4.35}$$

The corrected model $\hat{G}$ then can be written as:

$$\hat{G}(s) \;=\; G_N(s) + K. \tag{4.36}$$

The matrix $K \in \mathbf{R}^{m\times n}$ is determined by finding K that minimizes the weighted error between the full-order model and the corrected model. The approach used here follows [Moh00b], where the cost function is defined similar to (4.4):

$$J \;=\; \|W(s)(G(s) - \hat{G}(s))\|_2^2 \tag{4.37}$$

and W is defined in (4.5).

Let

$$\tilde{G}(s) \;=\; \sum_{i=N+1}^{\infty} \frac{P_i}{s^2 + 2\zeta_i\omega_i s + \omega_i^2}. \tag{4.38}$$

Then, the cost function can be shown to be:

$$\begin{aligned} J \;&=\; \|W(s)(\tilde{G}(s) - K)\|_2^2 \\ &=\; \|W\tilde{G}\|_2^2 + \frac{1}{2\pi}\int_{-\omega_c}^{\omega_c} \mathrm{tr}\{K^T K\}d\omega - 2\times\frac{1}{2\pi}\int_{-\omega_c}^{\omega_c} \mathbf{Re}\{\mathrm{tr}\{\tilde{G}(j\omega)^* K\}\}d\omega. \end{aligned} \tag{4.39}$$

We differentiate the cost function J with respect to K to obtain the condition of optimality:

$$\frac{dJ}{dK} \;=\; 2\times 2\omega_c \times \frac{1}{2\pi}K_{opt} - 2\times\frac{1}{2\pi}\int_{-\omega_c}^{\omega_c} \mathbf{Re}\{\tilde{G}(j\omega)\}d\omega \;= 0. \tag{4.40}$$

Hence, the optimum value of K is

$$K_{opt} \;=\; \frac{1}{2\omega_c}\int_{-\omega_c}^{\omega_c} \mathbf{Re}\{\tilde{G}(j\omega)\}d\omega. \tag{4.41}$$

Using (4.41) and (4.38), the optimum feedthrough term K_{opt} is

$$K_{opt} \;=\; \frac{1}{2\omega_c}\int_{-\omega_c}^{\omega_c} \sum_{i=N+1}^{\infty} \frac{(\omega_i^2 - \omega^2)P_i}{(\omega_i^2 - \omega^2)^2 + 4\zeta_i^2\omega_i^2\omega^2}d\omega. \tag{4.42}$$

To evaluate the above expression, the integral needs to be solved first. Next, we will consider the case of spatial models first before we attempt to evaluate K_{opt}.

4.3.2 Problem statement for spatial models

Consider the spatial model of a resonant system with damping:

$$G_r(s,r) = \sum_{i=1}^{\infty} \frac{\phi_i(r)P_i}{s^2 + 2\zeta_i\omega_i s + \omega_i^2} \tag{4.43}$$

where $P_i \in \mathbf{R}^{1\times n}$ for a system with n inputs.

The truncated spatial model is

$$G_{rN}(s,r) = \sum_{i=1}^{N} \frac{\phi_i(r)P_i}{s^2 + 2\zeta_i\omega_i s + \omega_i^2}. \tag{4.44}$$

A feedthrough term $K_r \in \mathbf{R}^{1\times n}$ is added to the truncated model G_{rN}. The corrected model is

$$\hat{G}_r(s,r) = G_{rN}(s,r) + K_r(r) \tag{4.45}$$

and K_r is chosen in the form in (4.11).

K_{ri} is determined such that the spatial $\mathcal{H}_2$ norm of the weighted error between the full-order model (4.43) and the corrected model (4.45) is minimized. The approach follows [Moh00a], where the cost function is similar to (4.12):

$$\begin{aligned} J_r &= \ll W_r(s,r)(G_r(s,r) - \hat{G}_r(s,r)) \gg_2^2 \\ &= \ll W_r(s,r)(\tilde{G}_r(s,r) - K_r(r)) \gg_2^2 \end{aligned} \tag{4.46}$$

where

$$\tilde{G}_r(s,r) = \sum_{i=N+1}^{\infty} \frac{\phi_i(r)P_i}{s^2 + 2\zeta_i\omega_i s + \omega_i^2} \tag{4.47}$$

and W_r is defined in (4.14).

Then the cost function can be expanded as follows:

$$\begin{aligned} J_r &= \ll W_r(s,r)\tilde{G}_r(s,r) \gg_2^2 + \frac{1}{2\pi}\int_{-\omega_c}^{\omega_c}\int_{\mathcal{R}} \mathrm{tr}\{K_r(r)^T K_r(r)\} dr\, d\omega \\ &\quad -2\times\frac{1}{2\pi}\int_{-\omega_c}^{\omega_c}\int_{\mathcal{R}} \mathbf{Re}\{\mathrm{tr}\{\tilde{G}_r(j\omega,r)^* K_r(r)\}\} dr\, d\omega \\ &= \ll W_r(s,r)\tilde{G}_r(s,r) \gg_2^2 \\ &\quad +\frac{1}{2\pi}\int_{-\omega_c}^{\omega_c}\int_{\mathcal{R}} \mathrm{tr}\left\{\left(\sum_{i=N+1}^{\infty}\phi_i(r)K_{ri}^T\right)\times\left(\sum_{l=N+1}^{\infty}\phi_l(r)K_{rl}\right)\right\} dr\, d\omega \\ &\quad -2\times\frac{1}{2\pi}\int_{-\omega_c}^{\omega_c}\int_{\mathcal{R}} \mathbf{Re}\left\{\mathrm{tr}\left\{\left(\sum_{i=N+1}^{\infty}\frac{\phi_i(r)P_i^T}{(\omega_i^2-\omega^2)-2\zeta_i\omega_i j\omega}\right)\right.\right. \\ &\quad \left.\left.\times\left(\sum_{l=N+1}^{\infty}\phi_l(r)K_{rl}\right)\right\}\right\} dr\, d\omega. \end{aligned} \tag{4.48}$$

We use the orthogonality property of the eigenfunctions ϕ_i in (3.6) to obtain

$$\begin{aligned} J_r &= \ll W_r(s,r)\tilde{G}_r(s,r) \gg_2^2 + 2\omega_c\times\frac{1}{2\pi}\times\mathrm{tr}\left\{\sum_{i=N+1}^{\infty}K_{ri}^T K_{ri}\right\} \\ &\quad -2\times\frac{1}{2\pi}\int_{-\omega_c}^{\omega_c}\mathbf{Re}\left\{\mathrm{tr}\left\{\sum_{i=N+1}^{\infty}\frac{P_i^T K_{ri}}{(\omega_i^2-\omega^2)-2\zeta_i\omega_i j\omega}\right\}\right\} d\omega. \end{aligned} \tag{4.49}$$

Obtaining the derivative of J_r with respect to K_{ri} gives the condition of optimality:

$$\begin{aligned} \frac{dJ_r}{dK_{ri}} &= 2\times 2\omega_c\times\frac{1}{2\pi}K_{ri}^{opt} - 2\times\frac{1}{2\pi}\int_{-\omega_c}^{\omega_c}\mathbf{Re}\left\{\frac{P_i}{(\omega_i^2-\omega^2)-2\zeta_i\omega_i j\omega}\right\} d\omega \\ &= 0. \end{aligned} \tag{4.50}$$

Hence, the optimal feedthrough K_{ri}^{opt} is

$$K_{ri}^{opt} = \frac{1}{2\omega_c}\int_{-\omega_c}^{\omega_c}\frac{(\omega_i^2-\omega^2)P_i}{(\omega_i^2-\omega^2)^2+4\zeta_i^2\omega_i^2\omega^2}d\omega. \tag{4.51}$$

It should be noticed that the optimal solution of the spatial case K_{ri}^{opt} in (4.51) involves the same integral as that of the pointwise case K^{opt} in (4.42). Hence, we only need to evaluate the integral to solve for both optimal solutions once.

The derivations of the integral can be found in Appendix A. The integral can be shown to be:

$$\begin{aligned} L &= \int_{-\omega_c}^{\omega_c}\frac{\omega_i^2-\omega^2}{(\omega_i^2-\omega^2)^2+4\zeta_i^2\omega_i^2\omega^2}d\omega \\ &= \frac{1}{2\omega_i\sqrt{1-\zeta_i^2}}\ln\left(\frac{\omega_c^2+2\omega_c\omega_i\sqrt{1-\zeta_i^2}+\omega_i^2}{\omega_c^2-2\omega_c\omega_i\sqrt{1-\zeta_i^2}+\omega_i^2}\right). \end{aligned} \tag{4.52}$$

After obtaining the solution for the integral, we can now determine the optimal feedthrough terms for both pointwise and spatial models.

4.3.3 Pointwise models, K_{opt}

From (4.52), the solution for K_{opt} for pointwise models (4.42) is

$$\begin{aligned} K_{opt} &= \frac{1}{2\omega_c}\sum_{i=N+1}^{\infty}\int_{-\omega_c}^{\omega_c}\frac{(\omega_i^2-\omega^2)P_i}{(\omega_i^2-\omega^2)^2+4\zeta_i^2\omega_i^2\omega^2}d\omega \\ &= \frac{1}{4\omega_c}\sum_{i=N+1}^{\infty}\frac{1}{\omega_i\sqrt{1-\zeta_i^2}}\ln\left(\frac{\omega_c^2+2\omega_c\omega_i\sqrt{1-\zeta_i^2}+\omega_i^2}{\omega_c^2-2\omega_c\omega_i\sqrt{1-\zeta_i^2}+\omega_i^2}\right)P_i. \quad (4.53) \end{aligned}$$

We now compare the above solution with the optimal solution with no damping effect. From (4.7), if $\zeta_i = 0$, $\forall i$, then $K_{opt} = \frac{1}{2\omega_c}\sum_{i=N+1}^{\infty}\frac{1}{\omega_i}\ln\left(\frac{\omega_i+\omega_c}{\omega_i-\omega_c}\right)P_i$. It can be observed that

$$\ln\left(\frac{\omega_c^2+2\omega_c\omega_i\sqrt{1-\zeta_i^2}+\omega_i^2}{\omega_c^2-2\omega_c\omega_i\sqrt{1-\zeta_i^2}+\omega_i^2}\right) \rightarrow 2\ln\left(\frac{\omega_i+\omega_c}{\omega_i-\omega_c}\right) \text{ as } \quad \zeta_i \rightarrow 0. \quad (4.54)$$

Hence,

$$K_{opt} \rightarrow \frac{1}{2\omega_c}\sum_{i=N+1}^{\infty}\frac{1}{\omega_i}\ln\left(\frac{\omega_i+\omega_c}{\omega_i-\omega_c}\right)P_i \text{ as } \quad \zeta_i \rightarrow 0 \quad (4.55)$$

The optimal solution determined here is consistent with the solution when no damping is assumed.

4.3.4 Spatial models, K_{ri}^{opt}

Similarly for spatial models, the optimal feedthrough term is

$$K_r^{opt}(r) = \sum_{i=N+1}^{\infty}\phi_i(r)K_{ri}^{opt} \quad (4.56)$$

with

$$\begin{aligned} K_{ri}^{opt} &= \frac{1}{2\omega_c}\int_{-\omega_c}^{\omega_c}\frac{(\omega_i^2-\omega^2)P_i}{(\omega_i^2-\omega^2)^2+4\zeta_i^2\omega_i^2\omega^2}d\omega \\ &= \frac{1}{4\omega_c\omega_i\sqrt{1-\zeta_i^2}}\ln\left(\frac{\omega_c^2+2\omega_c\omega_i\sqrt{1-\zeta_i^2}+\omega_i^2}{\omega_c^2-2\omega_c\omega_i\sqrt{1-\zeta_i^2}+\omega_i^2}\right)P_i. \quad (4.57) \end{aligned}$$

From (4.16), the solution for $\zeta_i = 0, \forall i$ is $K_{ri}^{opt} = \frac{1}{2\omega_c\omega_i} \ln\left(\frac{\omega_i+\omega_c}{\omega_i-\omega_c}\right) P_i$. Comparing the solution in (4.57) with that for the no damping case, it can be verified that

$$K_{ri}^{opt} \quad \rightarrow \quad \frac{1}{2\omega_c\omega_i} \ln\left(\frac{\omega_i+\omega_c}{\omega_i-\omega_c}\right) P_i \quad \text{as } \zeta_i \rightarrow 0. \tag{4.58}$$

Hence, the correction term for the spatial model presented above, approaches to the case with no damping reported in [Moh00a].

The solutions in (4.53) and (4.57) contain ω_i in their denominators. Hence, the contribution of each mode to the solutions tends to decrease as i increases. Therefore, it is sufficient to include a sufficiently large number of the out-of-bandwidth modes to calculate these optimal feedthrough terms.

Next, we will demonstrate the effectiveness of our proposed model correction solutions in compensating for truncation error. In particular, we want to show that when the system has damping in it, our solutions can be expected to perform better than those that ignore the damping effect (proposed in [Moh00a, Moh00b], see Sections 4.1.1 and 4.1.2).

For each mode i, the contribution to the feedthrough term in (4.53) and (4.56) is proportional to

$$k_i \quad = \quad \frac{1}{\omega_i\sqrt{1-\zeta_i^2}} \ln\left(\frac{\omega_c^2 + 2\omega_c\omega_i\sqrt{1-\zeta_i^2} + \omega_i^2}{\omega_c^2 - 2\omega_c\omega_i\sqrt{1-\zeta_i^2} + \omega_i^2}\right). \tag{4.59}$$

We express the resonance frequency as $\omega_i = k_{\omega i}\omega_c$, so k_i may be re-written as:

$$k_i \quad = \quad \frac{1}{k_{\omega i}\omega_c\sqrt{1-\zeta_i^2}} \ln\left(\frac{1 + 2k_{\omega i}\sqrt{1-\zeta_i^2} + k_{\omega i}^2}{1 - 2k_{\omega i}\sqrt{1-\zeta_i^2} + k_{\omega i}^2}\right). \tag{4.60}$$

The normalized k_i is then obtained by dividing k_i (4.60) with the arbitrary reference k_i that is evaluated at $\zeta_i = 0, k_{\omega i} = 1.5$. The reference value is used so k_i is independent of the actual value of ω_i.

The resonance frequency of mode i is normalized with respect to the cut-off frequency, i.e. ω_i/ω_c. The normalized k_i changes as the damping ratio and normalized resonance frequency are varied as shown in Figure 4.6. At large

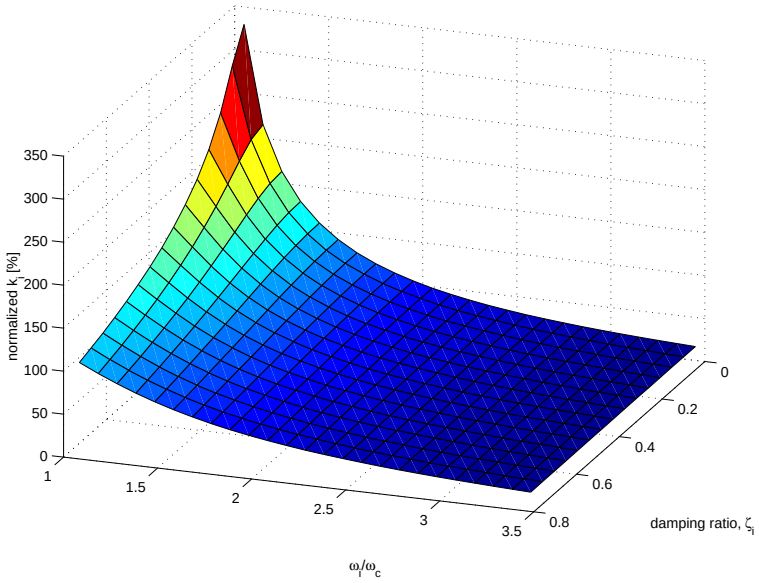

Figure 4.6: The normalized k_i

ω_i/ω_c ratio, the effect of damping on the normalized k_i is minimal. There is small difference between the results with and without the damping effect. However, at smaller ω_i/ω_c ratio, the difference becomes more significant. This corresponds to the case of out-of-bandwidth modes that are close to the cut-off frequency ω_c. When the resonance frequency is relatively close to the cut-off frequency, the feedthrough term will give an excessive value if the damping effect is ignored. This is expected as when ω_i is close to ω_c, the effect of damping of that mode on the in-bandwidth dynamics is considerable. For the case where damping is ignored, the normalized k_i will have an infinite value when $\omega_i/\omega_c = 1$. Therefore, it is necessary to include the damping effect especially for the out-of-bandwidth modes that are close to ω_c.

4.4 Illustrative example

We now consider applying our model correction solutions to a specific example, a simply-supported flexible structure. The structure is a 60 cm long uni-

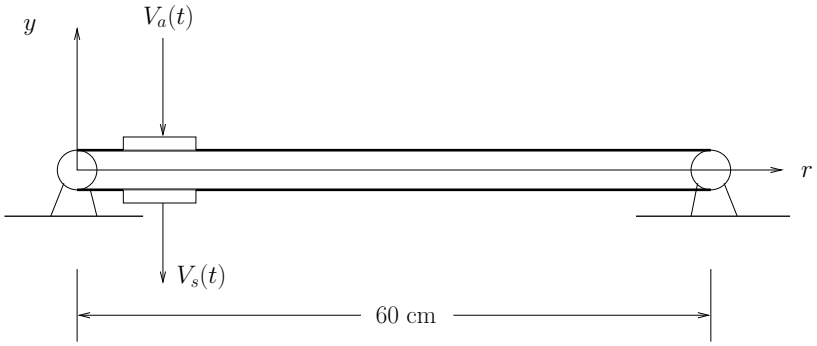

Figure 4.7: A simply-supported beam

Beam length, L	0.600 m
Beam width, W	0.050 m
Beam thickness, h	0.003 m
Beam Young's modulus, E	7.00×10^{10} N/m^2
Beam density, ρ	2.770×10^{3} kg/m^3
Piezoceramic r-length, L_p	0.070 m
Piezoceramic width, W_p	0.025 m
Piezoceramic thickness, h_p	2.50×10^{-4} m
Piezoceramic Young's modulus, E_p	6.70×10^{10} N/m^2
Charge constant, d_{31}	-2.10×10^{-10} m/V
Voltage constant, g_{31}	-1.15×10^{-2} Vm/N
Capacitance, C	1.05×10^{-7} F
Electromechanical coupling factor, k_{31}	0.34

Table 4.2: Properties of the piezoelectric laminate beam

form aluminium beam of a rectangular cross section as shown in Figure 4.7. A pair of piezoelectric ceramic elements is attached symmetrically to either side of the beam, 50 mm away from one end of the beam. The piezoceramic elements used are PIC151 patches. Some properties of the piezoelectric laminate beam are shown in Table 4.2.

Modal analysis is used to obtain pointwise and spatial models of the beam. The pointwise model used is the transfer function from the piezoelectric actuator voltage V_a to its collocated sensor voltage V_s. The spatial model is the transfer function from the piezoelectric actuator voltage to the transverse deflection y at any point along the beam. The simulation results are presented below. The damping factor associated with each mode is assumed to be $\zeta_i = 0.025$ in this simulation. We include the first eleven modes as the in-bandwidth modes, and higher modes up to mode 100 as the out-of-bandwidth modes. The out-of-bandwidth modes will be used to calculate the optimal feedthrough term. The first 100 modes are considered sufficient since including higher modes does not change the in-bandwidth dynamics significantly. The cut-off frequency is $\omega_c = 2,682$ Hz, which is between modes 11 and 12.

4.4.1 Pointwise model

Figure 4.8 compares the zeros of the truncated and full-order models up to the frequency ω_c. The full-order model consists of modes from 1 to 100. Similar to the case in Section 4.2, there are errors in the locations of zeros of the truncated model due to removal of out-of-bandwidth modes. Figure 4.9 demonstrates the effect of adding the optimal feedthrough term to the truncated model, where the errors in the locations of zeros of the compensated model are reduced substantially. The improvement of the compensated model can also be seen by comparing Figures 4.10 and 4.11. Here, the error in DC content of the truncated model in Figure 4.10 is reduced by adding the feedthrough term as shown in Figure 4.11.

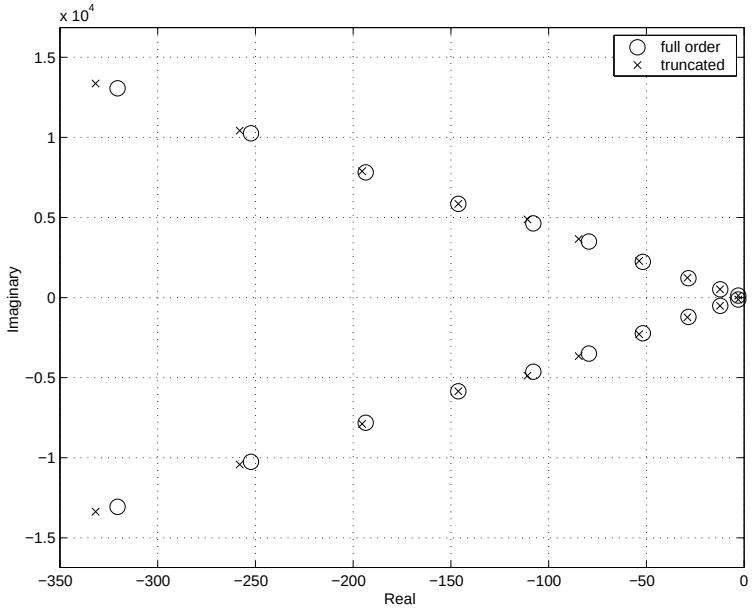

Figure 4.8: Zeros of full-order and truncated models

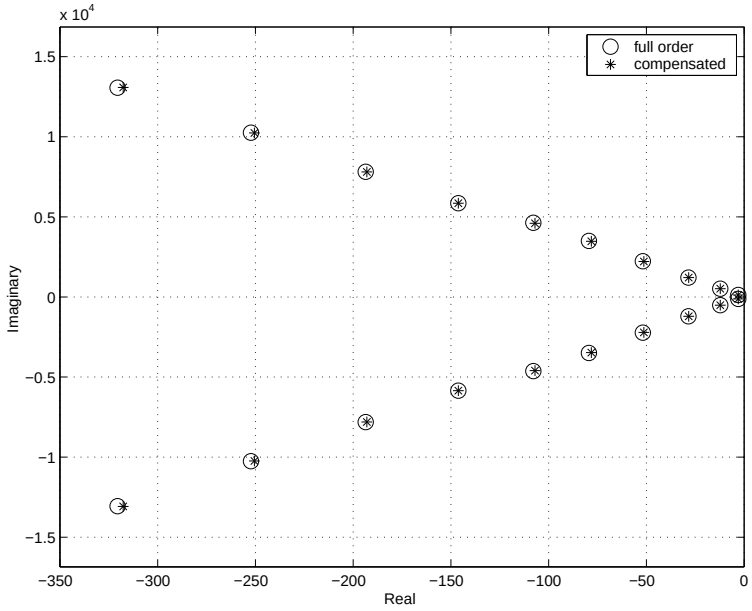

Figure 4.9: Zeros of full-order and corrected models

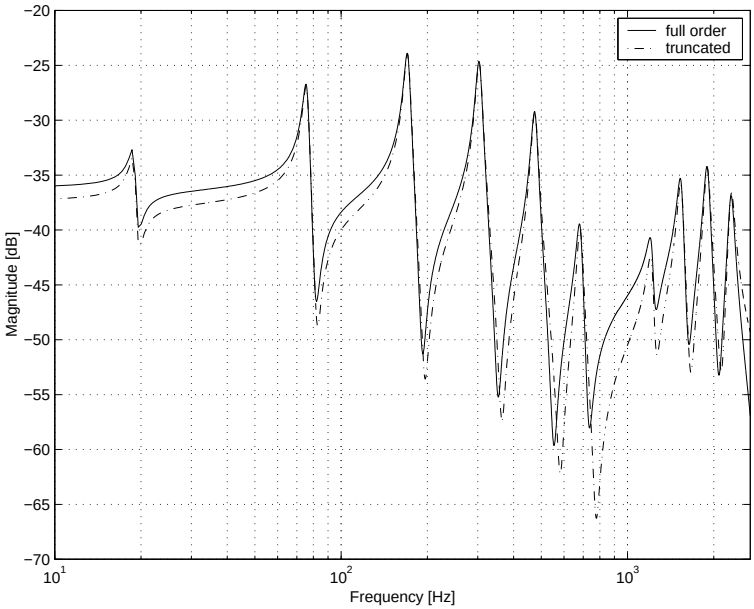

Figure 4.10: Full-order and truncated models

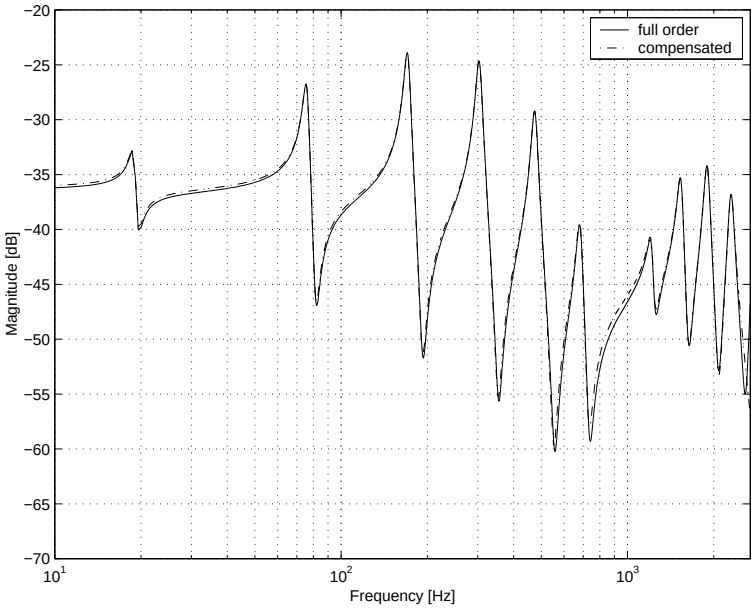

Figure 4.11: Full-order and corrected models

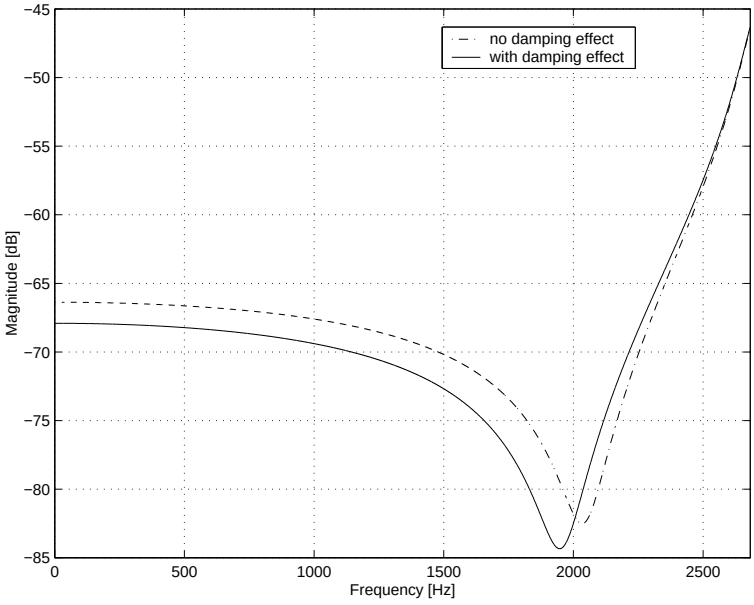

Figure 4.12: Frequency responses of error systems

The frequency responses (magnitude) of the error systems corresponding to both approaches are presented in Figure 4.12. The error system is based on the error of the corrected model with respect to the full-order model. The first error system is based on the approach that ignores the damping effect [Moh00b], while the second is based on our approach that incorporates the damping effect. The second approach has a smaller error at low frequencies, while the first approach has a smaller error at high frequencies. At frequencies near ω_c, both approaches yield similar errors. However, it can be observed that our approach performs better in most in-bandwidth frequencies. A better performance is expected when the system damping is considerable.

4.4.2 Spatial model

The performance of the proposed approach in compensating for the truncation error of a spatial system can be seen from Figures 4.13, 4.14, 4.15, and 4.16. The figures show the frequency responses (magnitude) of error systems at

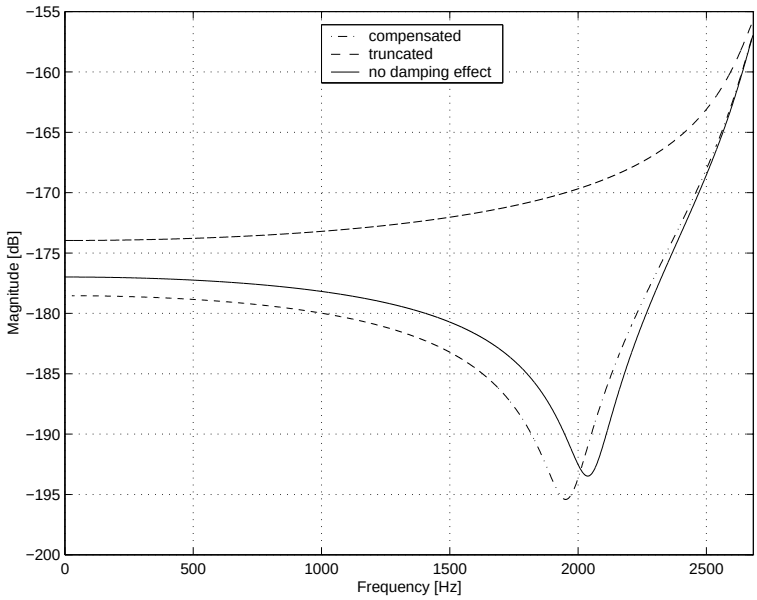

Figure 4.13: Frequency responses of error systems at r=0.13m

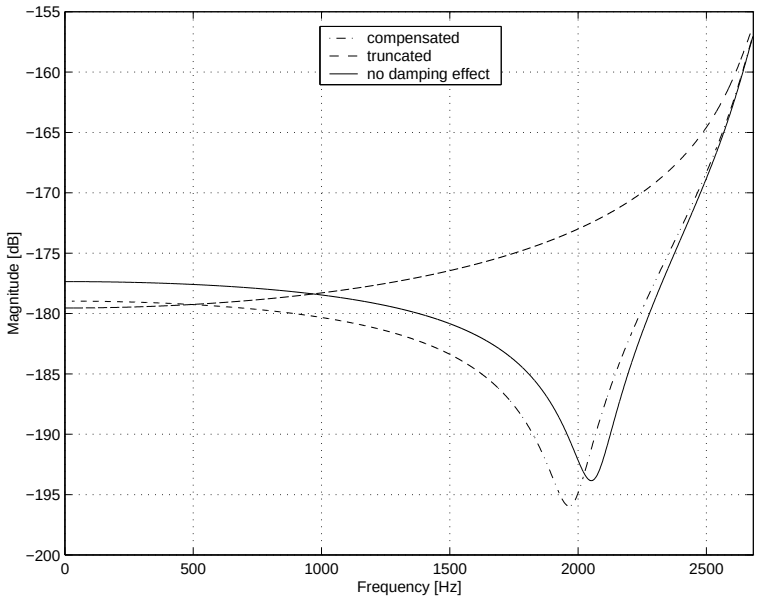

Figure 4.14: Frequency responses of error systems at r=0.27m

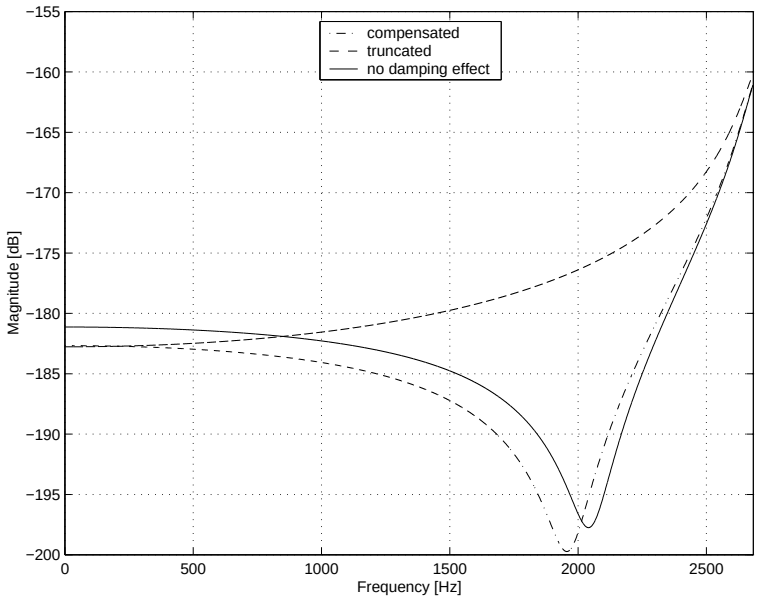

Figure 4.15: Frequency responses of error systems at r=0.36m

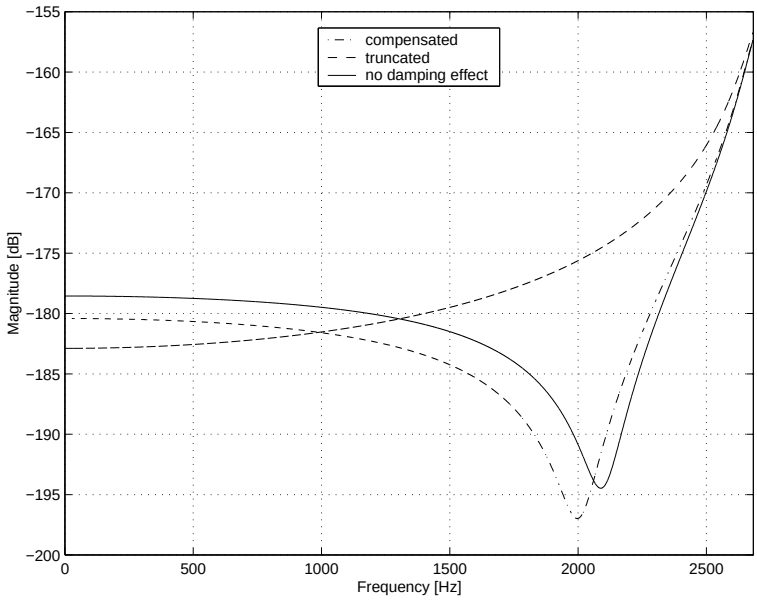

Figure 4.16: Frequency responses of error systems at r=0.47m

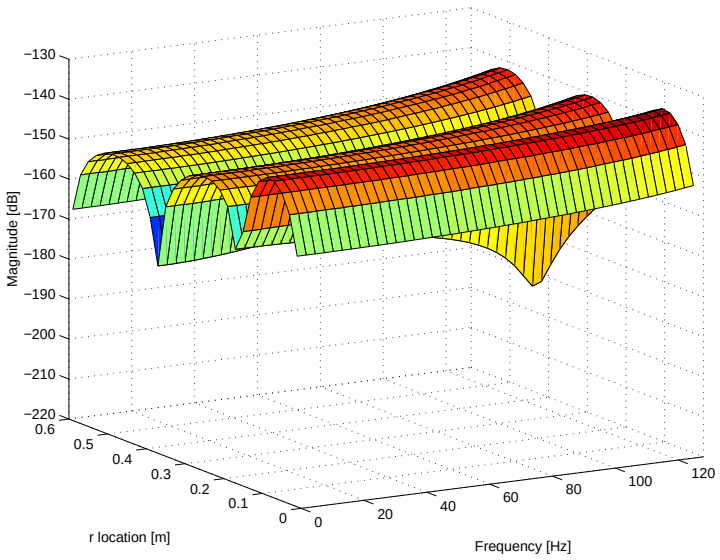

Figure 4.17: Spatial error frequency response for the truncated model

four different locations along the beam ($r = 0.13,\ 0.27,\ 0.36$ and 0.47 m). The magnitudes of error systems for truncated models, and corrected models with and without the damping effect are shown in the plots. Similar to the case of pointwise models, our approach performs better in a wide range of in-bandwidth frequencies than the approach with no damping effect in [Moh00a].

However, at some locations along the beam (e.g. $r = 0.27, 0.47$ m), the error at low frequencies for the corrected model exceeds that of the truncated model. The reason is that the feedthrough term is optimized by minimizing the spatial $\mathcal{H}_2$ norm of the error system. Hence, it is possible that a larger error may result at some locations on the structure over some frequency range. However, the overall spatial error of the corrected model will be minimum. In some resonant systems with considerable damping such as acoustic systems [MFM02], the advantage of our proposed approach over the previous approach will be more significant.

In order to demonstrate the effect of adding the optimal feedthrough term more clearly, we consider the first two modes as in-bandwidth modes. The out-

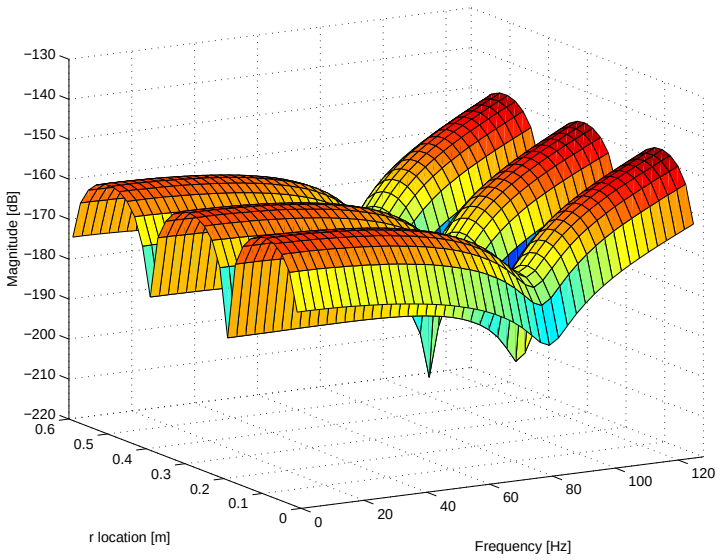

Figure 4.18: Spatial error frequency response for the corrected model

of-bandwidth modes consist of mode 3 to mode 100 and the cut-off frequency is $\omega_c = 128$ Hz. The spatial error frequency responses (magnitude) for the truncated and corrected models are plotted in Figures 4.17 and 4.18 respectively. The error of the truncated model increases with frequency, while the error of the corrected model decreases to a minimum at the mid-frequency region. From the plots, the error of the truncated model ranges from -180 dB to -136 dB spatially, while the error of the corrected model ranges from -210 dB to -146 dB spatially. It is obvious that the corrected model has a generally smaller error over the entire structure.

Finally, we compare pointwise frequency responses at several locations along the beam ($r = 0.10,\ 0.21$ and 0.42 m) in Figures 4.19, 4.20, and 4.21 respectively. The results show the effectiveness of the proposed approach in compensating for the truncation error spatially.

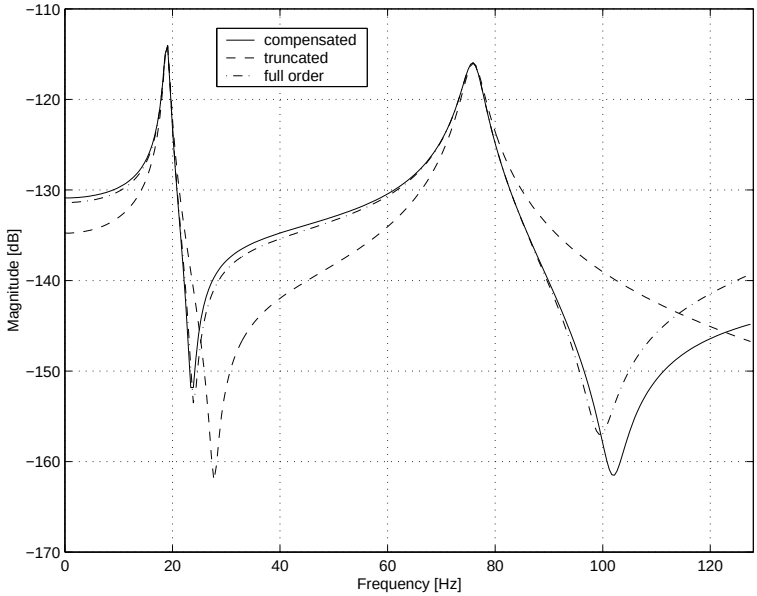

Figure 4.19: Pointwise frequency responses at r=0.10m

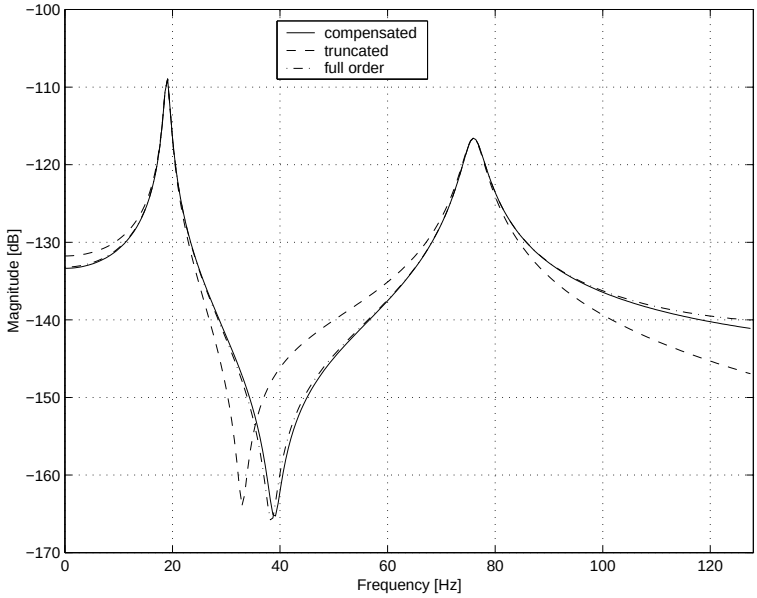

Figure 4.20: Pointwise frequency responses at r=0.21m

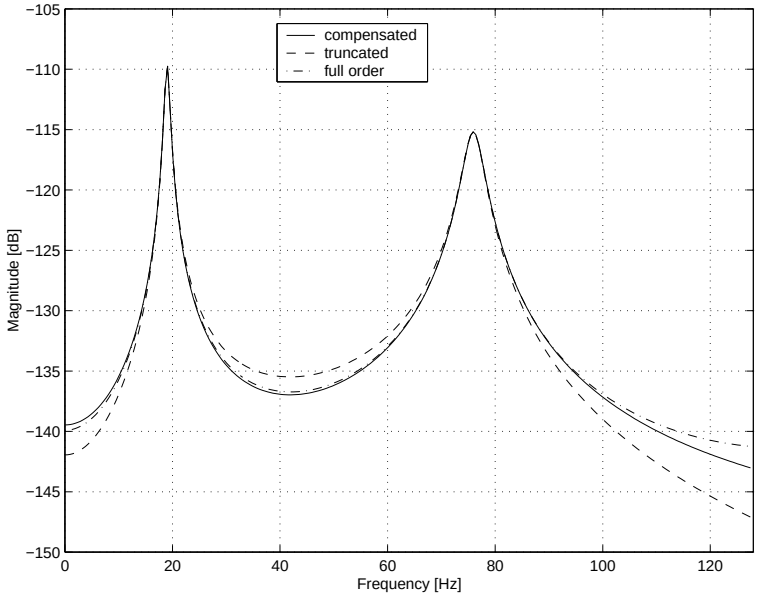

Figure 4.21: Pointwise frequency responses at r=0.42m

4.5 Model correction for models from approximate methods

When a model is obtained from an approximate method, we can ask how to compensate for such a model. The model consists of a finite number of modes, which differs from models obtained from modal analysis. However, it may be necessary to reduce the order of the model for control design purposes.

In pointwise cases, the model correction approaches described in Sections 4.2 and 4.3.1 can be used. However, the model correction approach in Section 4.3.2 cannot be used for spatial cases. The difficulty in applying the previous approach for spatial cases is because of the orthogonality condition that is assumed for eigenfunctions in (3.6). This orthogonality condition assumes a structure with a uniform mass distribution. In more general cases of flexible structures, the eigenfunctions are, in fact, orthogonal with respect to the associated distributed mass as implied by (2.44).

This section will extend the model correction methodology for spatial models that are obtained from approximate methods. Initially, we consider the case of models that are developed via the FE method. In particular, we consider a model of the beam that was discussed in Chapter 2.

Consider a spatial system obtained from the the FE method in (2.111):

$$G_r(s,r) \;=\; \sum_{i=1}^{k} \frac{C_w(r)\,\phi_i\,\phi_i^T\,\bar{F}}{s^2+2\zeta_i\omega_i s+\omega_i^2}.$$

Definition 4.1 Distributed mass: *Considering the FE beam in Section 2.7, suppose ρ_{bn} and A_{bn} are the density and cross-sectional area of the n^{th} element. The distributed mass of the beam with N elements is defined as:*

$$m(r) \;=\; \rho_{bn}A_{bn} \qquad for \quad (n-1)h_e < r < nh_e \qquad n=1,\ldots,N. \quad (4.61)$$

Lemma 4.2 *Considering the distributed mass $m(r)$ in Definition 4.1 and $C_w(r)$ in (2.96), the eigenvector ϕ_i is orthogonal with respect to $\int_0^L C_w(r)^T m(r) C_w(r) dr$:*

$$\phi_i^T \int_0^L C_w(r)^T\, m(r)\, C_w(r)\, dr\, \phi_p \;=\; \delta_{ip} \quad (4.62)$$

where δ_{ip} is the Kronecker delta function.

Proof *Using the expression for C_w (2.96) and realizing that the n^{th} elemental mass matrix is $M_{en} = \rho_{bn}A_{bn}\int_0^{h_e} \bar{H}(r_e)\bar{H}(r_e)^T dr_e$ in (2.93), then*

$$\begin{aligned}
\int_0^L C_w(r)^T\, m(r)\, C_w(r) dr \;&=\; \sum_{n=1}^{N} \int_0^{h_e} C_w(r_e)^T\, m(r_e)\, C_w(r_e) dr_e \\
&=\; \sum_{n=1}^{N} A_n^T \left(\int_0^{h_e} \bar{H}(r_e)\, \rho_{bn}A_{bn}\, \bar{H}(r_e)^T\, dr_e \right) A_n \\
&=\; \sum_{n=1}^{N} A_n^T\, M_{en}\, A_n \\
&=\; \hat{M}.
\end{aligned}$$

Since ϕ_i is orthonormal with respect to the mass matrix $\hat{M}$ (2.104), this completes the proof of the lemma.

Now, we can obtain the following theorem:

Theorem 4.1 *Consider the spatial system $G_r(s,r)$ in (2.111). The weighted spatial $\mathcal{H}_2$ norm of the system is*

$$\ll G_r(s,r) \gg_{2,m}^2 = \sum_{i=1}^{k} \|\tilde{G}_i(s)\|_2^2 \tag{4.63}$$

where m is the distributed mass and

$$\tilde{G}_i(s) = \frac{\phi_i^T \bar{F}}{s^2 + 2\zeta_i\omega_i s + \omega_i^2}. \tag{4.64}$$

Proof

$$\begin{aligned}
\ll G_r \gg_{2,m}^2 &= \frac{1}{2\pi}\int_{-\infty}^{\infty}\int_0^L tr\{G_r(j\omega,r)^*\, m(r)\, G_r(j\omega,r)\}\, dr\, d\omega \\
&= \frac{1}{2\pi}\int_{-\infty}^{\infty}\int_0^L tr\left\{\left(\sum_{i=1}^{k}\frac{\bar{F}^T\,\phi_i\,\phi_i^T\,C_w(r)^T}{(\omega_i^2-\omega^2)-2\zeta_i\omega_i j\omega}\right)\times m(r)\right. \\
&\quad \left.\times\left(\sum_{p=1}^{k}\frac{C_w(r)\,\phi_p\,\phi_p^T\,\bar{F}}{(\omega_p^2-\omega^2)+2\zeta_p\omega_p j\omega}\right)\right\} dr\, d\omega.
\end{aligned}$$

Using Lemma 4.2

$$\begin{aligned}
\ll G_r \gg_{2,m}^2 &= \frac{1}{2\pi}\int_{-\infty}^{\infty}\sum_{i=1}^{k} tr\left\{\frac{\bar{F}^T\phi_i}{(\omega_i^2-\omega^2)-2\zeta_i\omega_i j\omega}\times\frac{\phi_i^T\bar{F}}{(\omega_i^2-\omega^2)+2\zeta_i\omega_i j\omega}\right\} d\omega \\
&= \sum_{i=1}^{k}\|\tilde{G}_i(s)\|_2^2.
\end{aligned}$$

This completes the proof.

After establishing the theorem, we can consider the model correction of spatial models that are obtained from the FE method. Consider again the model G_r in (2.111). The corrected model is

$$\hat{G}_r(s,r) = G_{r\bar{k}}(s,r) + K_r(r) \tag{4.65}$$

where $\bar{k} < k$ and

$$G_{r\bar{k}}(s,r) = \sum_{i=1}^{\bar{k}}\frac{C_w(r)\,\phi_i\,\phi_i^T\,\bar{F}}{s^2+2\zeta_i\omega_i s+\omega_i^2}. \tag{4.66}$$

Here, K_r is chosen in the following form:

$$K_r(r) = \sum_{i=\bar{k}+1}^{k} C_w(r)\phi_i K_{ri}. \tag{4.67}$$

Instead of cost function in (4.46), we use the following cost function:

$$\begin{aligned} J_r &= \ll W_r(s,r)(G_r(s,r) - \hat{G}_r(s,r)) \gg_{2,m}^2 \\ &= \ll W_r(s,r)(\tilde{G}_r(s,r) - K_r(r)) \gg_{2,m}^2 \end{aligned} \tag{4.68}$$

where

$$\tilde{G}_r(s,r) = \sum_{i=\bar{k}+1}^{k} \frac{C_w(r)\phi_i\phi_i^T\bar{F}}{s^2 + 2\zeta_i\omega_i s + \omega_i^2} \tag{4.69}$$

and W_r has been defined previously in (4.14).

The cost function in (4.68) can be shown to be:

$$\begin{aligned} J_r &= \ll W_r(s,r)\tilde{G}_r(s,r) \gg_{2,m}^2 + \frac{1}{2\pi}\int_{-\omega_c}^{\omega_c}\int_0^L \mathrm{tr}\{K_r(r)^T m(r) K_r(r)\} dr\, d\omega \\ &\quad -2 \times \frac{1}{2\pi}\int_{-\omega_c}^{\omega_c}\int_0^L \mathbf{Re}\{\mathrm{tr}\{\tilde{G}_r(j\omega,r)^* m(r) K_r(r)\}\} dr\, d\omega \\ &= \ll W_r(s,r)\tilde{G}_r(s,r) \gg_{2,m}^2 \\ &\quad + \frac{1}{2\pi}\int_{-\omega_c}^{\omega_c}\int_0^L \mathrm{tr}\left\{\left(\sum_{i=\bar{k}+1}^{k} K_{ri}^T\phi_i^T C_w(r)^T\right) \times m(r) \right. \\ &\quad \left. \times \left(\sum_{l=\bar{k}+1}^{k} C_w(r)\phi_l K_{rl}\right)\right\} dr\, d\omega \\ &\quad -2 \times \frac{1}{2\pi}\int_{-\omega_c}^{\omega_c}\int_0^L \mathbf{Re}\left\{\mathrm{tr}\left\{\left(\sum_{i=\bar{k}+1}^{k} \frac{\bar{F}^T\phi_i\phi_i^T C_w(r)^T}{(\omega_i^2 - \omega^2) - 2\zeta_i\omega_i j\omega}\right) \times m(r) \right.\right. \\ &\quad \left.\left. \times \left(\sum_{l=\bar{k}+1}^{k} C_w(r)\phi_l K_{rl}\right)\right\}\right\} dr\, d\omega. \end{aligned} \tag{4.70}$$

Using the orthogonality property of the eigenvectors ϕ_i in Lemma 4.2 gives

$$\begin{aligned} J_r &= \ll W_r(s,r)\tilde{G}_r(s,r) \gg_{2,m}^2 + 2\omega_c \times \frac{1}{2\pi} \times \mathrm{tr}\left\{\sum_{i=\bar{k}+1}^{k} K_{ri}^T K_{ri}\right\} \\ &\quad -2 \times \frac{1}{2\pi}\int_{-\omega_c}^{\omega_c} \mathbf{Re}\left\{\mathrm{tr}\left\{\sum_{i=\bar{k}+1}^{k} \frac{\bar{F}^T\phi_i K_{ri}}{(\omega_i^2 - \omega^2) - 2\zeta_i\omega_i j\omega}\right\}\right\} d\omega. \end{aligned} \tag{4.71}$$

After obtaining the derivative of J_r with respect to K_{ri} as in Section 4.3.2, the optimal term K_{ri}^{opt} is

$$\begin{aligned} K_{ri}^{opt} &= \frac{1}{2\omega_c}\int_{-\omega_c}^{\omega_c} \frac{(\omega_i^2 - \omega^2)\phi_i^T\bar{F}}{(\omega_i^2 - \omega^2)^2 + 4\zeta_i^2\omega_i^2\omega^2} d\omega \\ &= \frac{1}{4\omega_c\omega_i\sqrt{1-\zeta_i^2}} \ln\left(\frac{\omega_c^2 + 2\omega_c\omega_i\sqrt{1-\zeta_i^2} + \omega_i^2}{\omega_c^2 - 2\omega_c\omega_i\sqrt{1-\zeta_i^2} + \omega_i^2}\right)\phi_i^T\bar{F} \end{aligned} \tag{4.72}$$

where the integral solution can be found from (4.52).

Similar results can be obtained from other approximate methods such as the Rayleigh-Ritz and assumed-modes methods. It can be shown, as outlined in [Mei75], that the estimated eigenfunctions are also orthogonal with respect to the distributed mass. These results give a more general model reduction methodology for spatial models since many systems cannot be modelled by modal analysis alone.

4.6 Summary

A number of different approaches can be used to compensate for the truncation error in models of resonant systems. The previous approaches assume no damping in the models since it simplifies the problems of finding the analytical optimal feedthrough terms. However, for systems with significant damping, the effect of damping may need to be included.

We extended the approach using the convex optimization and analytical approaches for finding the optimal feedthrough terms. The proposed analytical solutions generalize the previous solutions obtained with no-damping assumption. There is no limitation on the number of out-of-bandwidth modes that can be used in evaluating the feedthrough terms, since the terms can be readily computed from the analytical solutions. Therefore, the proposed solution provides a simple and effective way for model correction/reduction of pointwise and spatial systems.